Seismic Activity around Addis Ababa

A Thesis Submitted to School of Graduate Studies of Addis Ababa University In partial fulfillment of the requirements for the Degree of Master of Science in Solid Earth Geophysics

BY: MELESE TEMESGEN

School of Earth sciences

ADDIS ABABA UNIVERSITY

June 2018

Addis Ababa, Ethiopia

ADDIS ABABA UNIVERSITY

School of Earth sciences

Seismic Activity around Addis Ababa

BY: MELESE TEMESGEN

A Thesis Submitted to School of Graduate Studies of Addis Ababa University in partial fulfillment of the requirements for the Degree of Master of Sciences in Solid Earth Geophysics

ADDIS ABABA UNIVERSITY

June 2018

Addis Ababa, Ethiopia

ADDIS ABABA UNIVERSITY
School Of Graduate studies
School of Earth Sciences

This is to certify that the thesis prepared by Melese Temesgen entitled: "**Seismic Activity around Addis Ababa**" and submitted in partial fulfillment of the requirements for the Degree of Master of Science in Solid Earth Geophysics complies with the regulations of the University and meets the accepted standards with respect to originality and quality.

Approved by Examining Committee

Dr. Balemwal Atnafu Head, School of Earth Sciences	______________ Signature	_____________ Date
Dr. Atalay Ayele Advisor	______________ Signature	____________ Date
Prof. Tilahun Mammo Examiner	_____________ Signature	____________ Date
Dr. Elias Lewi Examiner	_____________ Signature	____________ Date

ACKNOWLEDGEMENT

I am deeply indebted to my advisor Dr. Atalay Ayele for providing me his time, to comment, guide and follow up the whole progress of this work. I have benefited immensely from his assistance, advice and encouragement throughout my study. I am also very grateful for his financial and material support during this work.

I also appreciate PhD students at IGSSA, Sisay Alemayehu and Jima Asefa for providing me with continuous technical support in familiarizing me with the softwares, giving me valuable comments and encouragement.

I would like to thank Dr. Shimiles Fessiha and Dr. Elias Lewi for their advice and encouragement in my courses and in whole of my study.

It is my pleasure to acknowledge and extend special thanks to staffs of Institute of Geophysics Space Science and Astronomy (IGSSA) specially Brehanu Abera, Tamirat Bekele and Daniel Mammo for their unlimited help and assistance in familiarizing me with the different software. They also have been helping me access seismological data and giving me their technical support in solving problems in computation.

Finally I also would like to appreciate my M.Sc classmates and my friends Habtamu Wagaw and Mesay Geletu for all the encouragement, advice and good times we have spent together.

ABSTRACT

All data recorded from January 2016 to August 2017 using the three permanently installed stations around the city namely AAE, FURI and ANKE together with the newly deployed (on December 2016) permanent seismic station WLRA (Wolmera) are used in this study. During this period81 natural earthquakes and 123 quarry explosions were recorded around Addis Ababa. The local magnitude of natural earthquakes registered ranges from 1.3 to 5.1 M_L and the local magnitude from quarry explosions ranges from 1.2 to 3.0 M_L.

The seismic events those from earthquakes clustered around the city of Addis Ababa. However, it is not in random fashion; most of the events from natural earthquakes around the city are concentrated following the trend of the MER which is NE -SW. Most of the epicenters concentrate SW and NE of the city. Few earthquake events are located on north of the city and around its eastern part. No events are located on the western part within the period of our observation.

The other seismic events registered are explosions from quarry sites in the neighborhood of Addis Ababa within 10-30 Km radius from the city center with the exception to the southwestern part. Epicenters from quarry explosion trend along the location of quarry sites. Most of the quarry events cluster east of the city since most of active quarry sites are located in that area; to be specific east of the Bole International Airport.

One of the discrimination methods of earthquakes from quarry blasts is by using origin time of events. Almost all quarry blasts are conducted in the daytime from 8:00AM to 5:00 PM whereas the natural earthquakes can originate anytime of the day. Locations of event sites are also used as a discriminator. Quarry sites, are clustered in close proximity to the city while natural earthquakes are not limited to specific sites and origin time unlike explosions.

The other method used for isolation of the two types of events is by comparing the spectra of the seismogram from natural earthquakes and from the quarry explosion. The spectrogram of events from natural earthquakes and quarry explosions is analyzed using the seismograms from Z component AAE and FURI for this study. The result shows a difference in frequency and energy radiation pattern for the two groups of events. The seismograms from quarry blasts have weaker body waves with high frequency content while earthquakes have stronger body wave arrival with low frequency content relative to the explosion events.

In addition I tried to discrimination events from quarry blasts and earthquakes by using ratio of amplitude of body waves to surfaces waves Ap/As. This method is not 100% efficient. However, I used it together with the above mentioned methods to discriminate quarry blasts from natural earthquakes.

Table of Contents

List of Tables

LISTS OF FIGURES

CHAPTER 1

INTRODUCTION

1.1. Background of the Study

The East African Rift System (EARS) bisects Ethiopia into two and the rift activity is manifested by the occurrence of tectonic earthquakes and active volcanism (Gouin 1979; Kebede, 1989; Abebe(2010), Ayele, 2017).

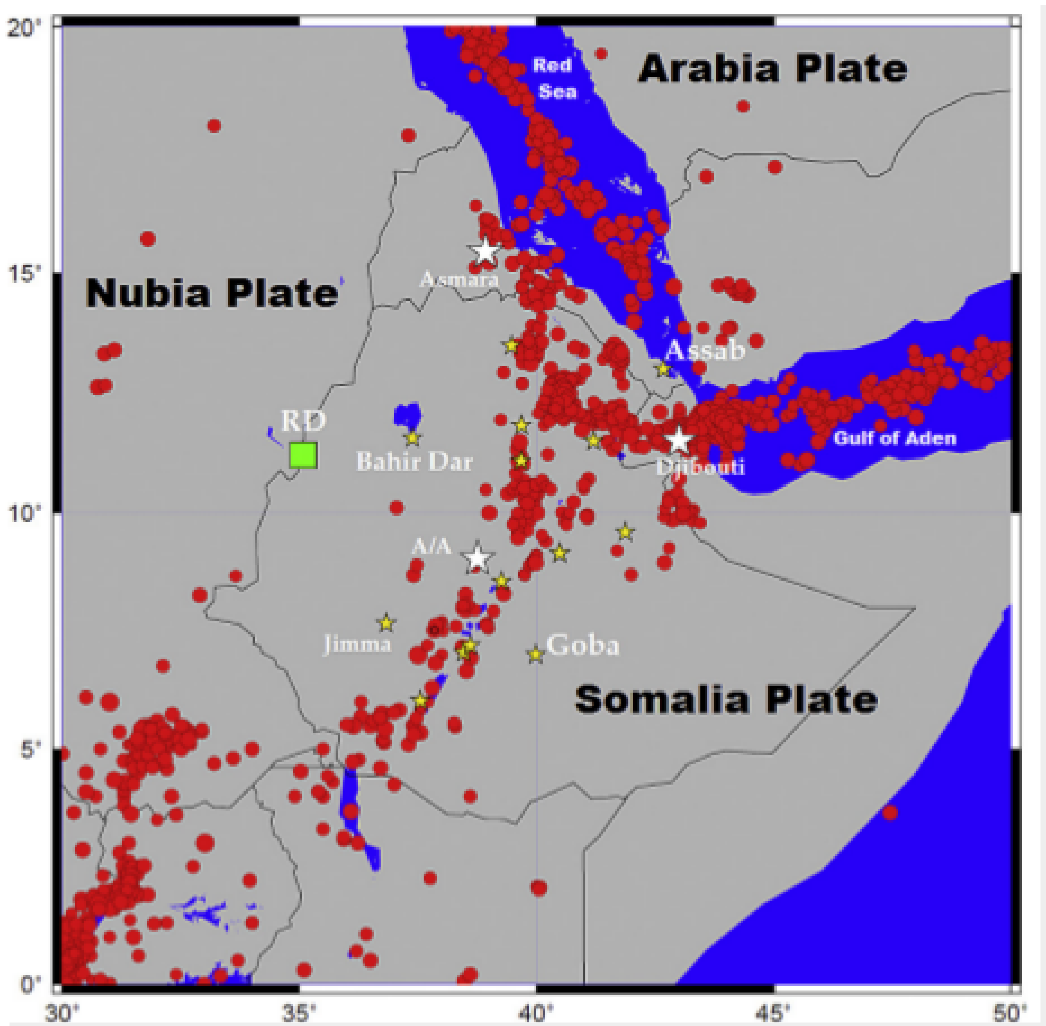

Figure 1.1 Seismicity of the Horn of Africa region for the period from 1900 to 2012 (Ayele, 2017).

The most significant earthquakes of the 20th century like the 1906 Langano earthquake, the 1961 Kara Kore earthquake, the 1983 Wondo Genet earthquake, the 1985 Langano earthquake, the 1989 Dobi graben earthquake in central Afar, and the 1993 Nazret earthquake were all felt in Addis Ababa, and the other major cities of Nazret and Awassa (Asfaw, 1992).

In area close to the proximity of Addis Ababa city, an estimated magnitude of about 6.5 ML earthquake is expected (Ababa RADIUS group, et al, 1999). In 1999, Ababa RADIUS group estimated that this earthquake could cause as many as 4000-5000 fatalities, 8000-10,000 injuries and evacuation of people as many as 500,000 and a total damage in excess of 12 Billion Birr (Ababa RADIUS group, et al, 1999). Considering the current population growth and infrastructure development in the capital city, the aforementioned figure may increase largely.

The problem of distinguishing the quarry blasts from natural earthquakes using seismic data has been studied for a long time ago. Currently, the discrimination of regional data is an important research topic and a variety of the regional discriminates have been proposed by many researchers. The discrimination of small magnitude events ($mb< 4$), the spectral discrimination using multiple regional phases has recently received much attention [Bennett & Murphy, 1986, Dahy, and Hassib, 2010).

There is a problem of identification of small earthquakes from quarry blasts where there are quarry sites around tectonically active areas.

Therefore the reasons for the study of seismicity around Addis Ababa are because Addis Ababa is

- Located on the western margin of tectonically active Main Ethiopian Rift (MER).
- The seat of African Union and other international organizations.
- One of the fast growing capital cities in infrastructure and population in Africa.

1.2 Location of the study area

The study area is located in central Ethiopia around Addis Ababa. Addis Ababa is located near the western margin of the Main Ethiopia Rift. It is bounded between 8°N to 11°N and 37°E to 40°E.

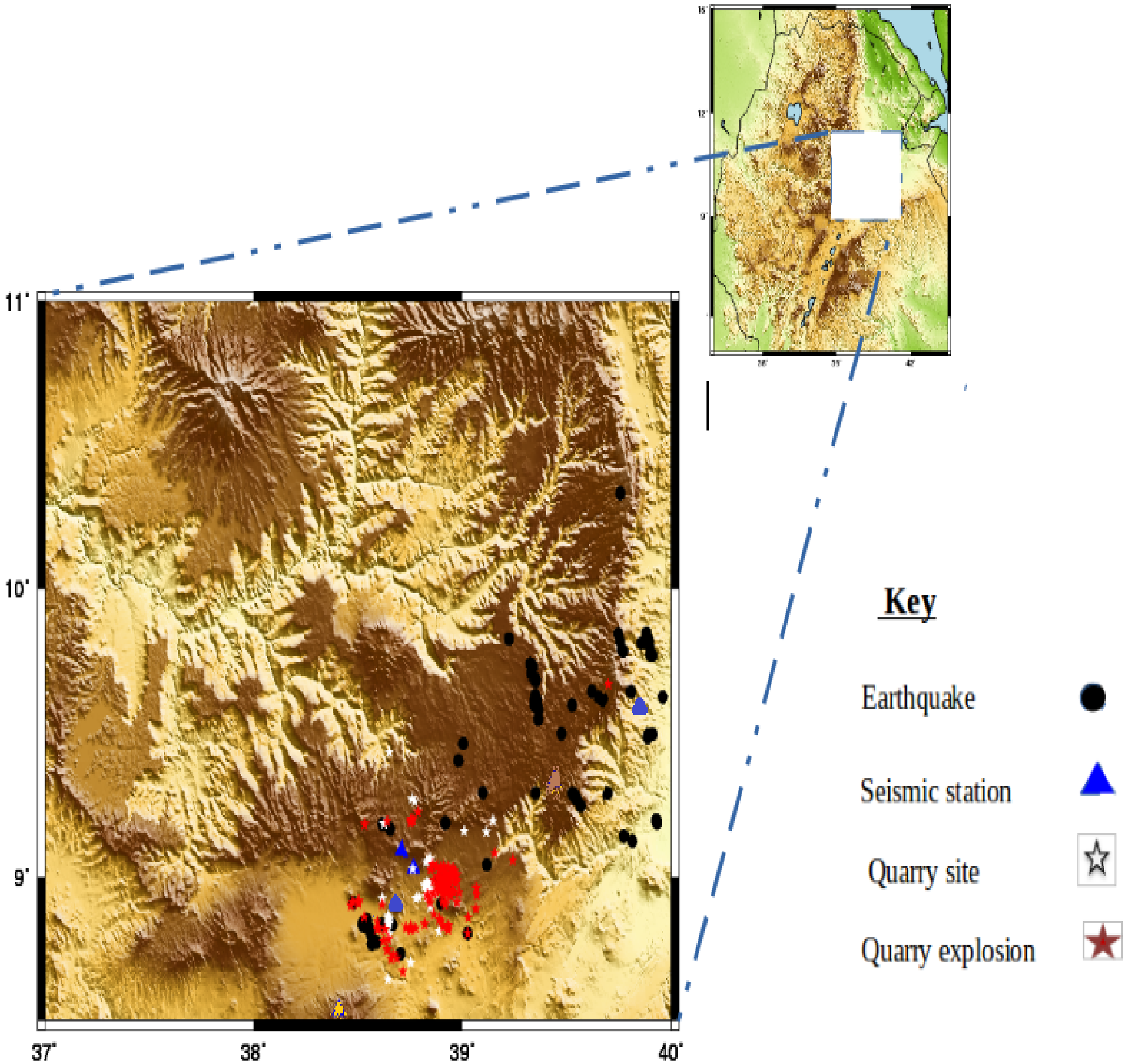

Figure 1.1 Topographic map of study area taken from GMT plotting of the locations of the area with the location of seismic stations used for this study.

1.3 Statement of the problem

Earthquakes of smaller magnitude are common in the neighborhood of Addis Ababa but are very difficult to identify whether they are natural earthquakes or quarry blasts. One of the main tasks of the Seismology and Earthquake Engineering unit under IGSSA is measuring the magnitude, locating and archiving earthquakes. However, the earthquake signal recorded from natural earthquakes is interfered by from quarry blasts going on a daytime around Addis Ababa, making it difficult to discriminate natural earthquakes from quarry explosions. Now the question is: how can we identify a natural earthquake if it occurs during daytime.

Therefore this study will solve this problem by finding a way to discriminate natural earthquakes from quarry explosions using the stations around Addis Ababa namely FURI station (On Mount Furi), AAE (A.A.U 4 kilo campus, in Addis Ababa university), WLRA (northwest of the city at Wolmera) and ANKE station about 150km east of Addis Ababa.

1.4 Objectives of the Study

1.4.1General Objectives

These seismic events due to explosions pose difficulty to seismologists at seismic observatories trying to catalog earthquake events, since they could be mistaken as local earthquakes. Therefore the objective of this work is to identify these quarry explosions events from natural earthquake seismic events.

1.4.2 Specific Objectives

The goal of this research is to

- Estimating the location (latitude, longitude, and depth) and origin time of events is by using the arrival times of various seismic phases picked from the recorded waveforms.
- Isolating natural earthquakes from quarry blasts by using their spatial and temporal distribution.
- Analyzing and comparing source spectra from earthquakes and explosions in and around Addis Ababa to develop new insights into discrimination methods between explosion and natural earthquake.
- Discriminating earthquakes from explosions using spectrogram method.
- Analyzing amplitude of body wave to surface wave Ap/As ratios as a function of frequency and evaluate different discrimination strategies

- Estimating the magnitudes of the earthquake or explosion

1.5 Significance of the Study

The significance of monitoring of the seismic activity around Addis Ababa is to help in making detailed and complete hazard map around Addis Ababa.

Monitoring the seismic activity help to detect artificial seismic sources (quarry blast and other cultural noises) and natural earthquakes, calculate the magnitude of these seismic events and spectral analysis of the waveforms of explosions and natural earthquakes.

The result of spectral analysis of the waveforms of from explosions and natural earthquakes help for seismologists who analyze earthquakes at observatories to discriminate easily between explosions and natural earthquakes.

1.5.1 Benefits of this study

- It is useful to show the sources of natural and artificial seismic activities around the city.
- It helps to determine magnitude of the seismic sources and the potential hazard to the city.
- It helps to know the distribution and frequency of seismic activities around the city.
- It helps to differentiate natural earthquakes from quarry explosions easily from the seismogram recording or from further analysis of the earthquake signals.

1.5.2 Limitation of the study

The study period is short for studying seismicity of Addis Ababa since the fourth station (WLRA) is deployed lately relative to other seismic stations and has shorter period to capture seismic events.

Lack of dense seismic station network around Addis Ababa makes studying the seismicity of the area difficult. The distribution of seismic stations around the city is not uniform. For example, the position of the ANKE seismic station that is found in Ankober town is the furthest from the city, which makes it out of the network of the other three stations around the city. This reduces the precision of event location using this station.

1.6 Literature Review

Addis Ababa is near the western edge of the Main Ethiopian Rift, which is a hotbed of tremors and active volcanoes. Some of Ethiopia's major cities like Addis Ababa, Adama, Dire Dawa and

Hawassa are very neart to the main fault lines such as the Wonji fault, the Nazret fault, the **Addis-Ambo-Ghedo** fault, and the **Fil Woha** fault lines along which numerous earthquakes of varying magnitude have occurred over the year's earthquake have been recorded. Other cities like Arba Minch, Dessie, and Mekele are also located in some of the most seismically active areas in the country. The presence of the Fil Woha hot springs in the middle of Addis Ababa itself, for example, is indicator that the city lies on fault lines that have been slowly building strains. The release of these strains on these faults accumulated over the years that cause earthquakes (Kinde, 2002).

Location	**Year**	**Magnitude**	**Distance of Epicenter from Addis (km)**	**Damage**
Langano	1906	6.8	110	Felt as far as Addis
Kara Kore	1961	6.7	150	Town of Majete destroyed. Kara Kore seriously damaged
Cenral Afar	1969			Town of Serdo destroyed
Wendo Genet	1983		300	
Langano	1985	6.2	110	
Rift Valley Area	1987	6.2	200	Widely felt and widely-spread damage.
Dobi [Central Afar]	1989	6.3	200	Several bridges damaged
Nazret	1993	6.0	< 100	Injuries and damage in Nazret. Also felt in D. Zeit and Addis.
	1997	4	22km	(source from, Haile, 2004, p.2).
Lake Shala – Adamitulu	1999		250	

Table 1.1 Summery of some of the recent significant earthquakes that have rocked the Rift Valley, the Afar Plains and the Western Edge of the Rift Valley sourced from (Guien,1979, Asfaw 1992)

In the past, several destructive earthquakes occurred in the region. These earthquakes were sometimes accompanied by light damages to some of the engineering structures within the city. Among the significant earthquakes which occurred within 200 km from the city are the 1906, the

1960, and the 1961 earthquakes of magnitudes 6.8, 6.3 and 6.7, respectively. The seismic activity is usually represented by small to intermediate size earthquakes. However, large size earthquake of magnitude 6.8 occurred in this zone in 1906 at an epicentral distance of about 120 km south of Addis Ababa. This was the largest earthquake ever that was recorded in Ethiopia. Its effect was widely felt in Addis Ababa. Other smaller magnitude earthquakes have occurred at closer range. The 1979 earthquake, with local magnitude of 4.1, occurred just 22 km southwest of the city, and another in 1974 with magnitude 4.6 happened about 100 km northeast of Addis Ababa. Both these caused great panic and inflicted some damage with intensities differing in different parts of the city (Gouin, 1979; Asfaw, 1990).

The epicenter map of the region shown in Fig. 1.2 shows that it is dominated by small and intermediate size earthquakes and that seismic activity in the region is not uniformly distributed but is characterized by clustering at preferred locations with sporadic activity in between them (Mammo, 2005).

Recently experts who participated in the RADIUS (Risk Assessment tools for Diagnosis of Urban areas against Seismic disasters) Project of Addis Ababa warned that earthquake of about the same size as those of the 1906 and 1961 earthquakes could occur at about 27 km away from the city. The RADIUS Project is an IDNDR (International Decade for Natural Disasters Reduction) initiative for the mitigation of the effects of major earthquakes in urban areas included Addis Ababa to be among the 9 case-study cities selected out of a total of 58 cities worldwide. In the wake of such an earthquake these experts estimated the resulting damages to the city—some 15% of buildings could suffer collapse and 19% severe damages leading to some 5000 deceased, 10,000 injured and 500,000 homeless people with more than 1.3 billion dollar worth damage in property (RADIUS, 1999). The study of the geology, tectonics and seismicity in the neighborhood of Addis Ababa shows a genetic relationship between faults and earthquake epicenters. Within the radius of 20–25 km to the south and east of the capital city swarms of NE–SW trending faults cut both Balchi rhyolites and the Bishoftu basalts. The orientation of the faults follows the regional trend of the faults in the Main Ethiopian Rift System. Similarly, trending faults within the city and to the immediate north cut the Basalts of Addis Ababa and the Entoto silicics, respectively. Farther north and northeast from the city, the faults cut the Termaber basalts and the Ashangi and Aiba basalts. The epicenters, plotted on the same map, are seen to follow the same strike as the faults and generally fall on the causative faults or on the extension of these faults. Most of the faults in the region have dimensions greater than 10 km. Within the city of Addis Ababa, the well-known Filwoha fault has an exposed length of more than 7 km. One fault about 20 km to the east of the city has an exposed length of about 30 km. Using the empirical relationships between fault lengths and earthquake magnitudes, and assuming that the rupturing took place all at once, the 30 km long fault rupture corresponds to an earthquake magnitude of about 6.8 (Hunt, 1984; Housner & Jennings, 1982).

The other most seismically active area around Addis Ababa is near Ankober, which in close proximity to Addis Ababa which is in the range of 150km (Ayele, 2010). According to Atalay Ayele it is very common to record single shocks and sequence of earthquakes frequently from the Ankober on AAE seismic station in the campus of Addis Ababa University. When we look at the seismic history of the area, it was shaken by 6.0 maximum magnitude earthquake in 1938 and onward then the tectonic stress is mostly released by smaller magnitude shocks. One of these recent seismic activities in the area is recorded on September 19, 2009 an earthquake of magnitude 5.0 Ml ruptured in an area 25 km northeast of the Ankober town at 17:56:07 GMT and this event was felt as far as Addis Ababa (Ayele, 2010).

Atalay Ayele, head of seismology and earthquake engineering unit in IGSSA (Institute of Geophysics Space Science and Astronomy) described the event as, “At the time of the event which is 9:00 local time many people were at home and it was widely felt in Addis specially residents who live on multistory buildings”. In addition, he suggested that other eminent earthquake damage is possible in the future in Addis Ababa unless decision makers and construction engineers take into consideration events such as this in planning and construction of structures.

The structural pattern of the area around Addis Ababa (Fig. 1.2) shows that the region, characterized by a complex fault pattern trending mainly around NE – SW, separates the Somalian Plate from the Nubian Plate.

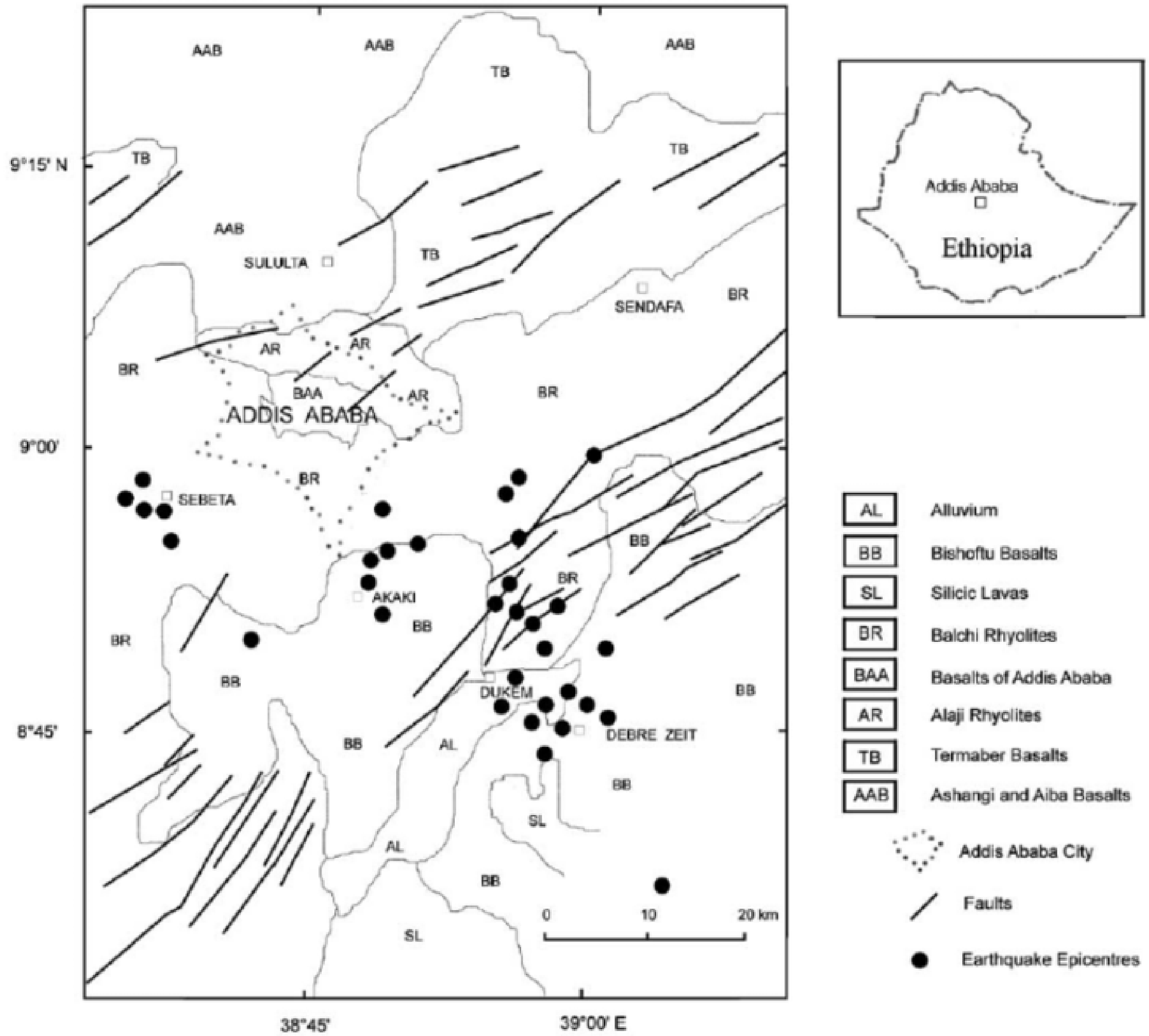

Figure 1.2 The geology, tectonic structures, and seismicity of the Addis Ababa (Mammo, 2005)

The histogram below shows a seismic gap following the 1984 earthquake in Addis Ababa, and large magnitude earthquake could happen in the near future releasing the seismic strain accumulated.

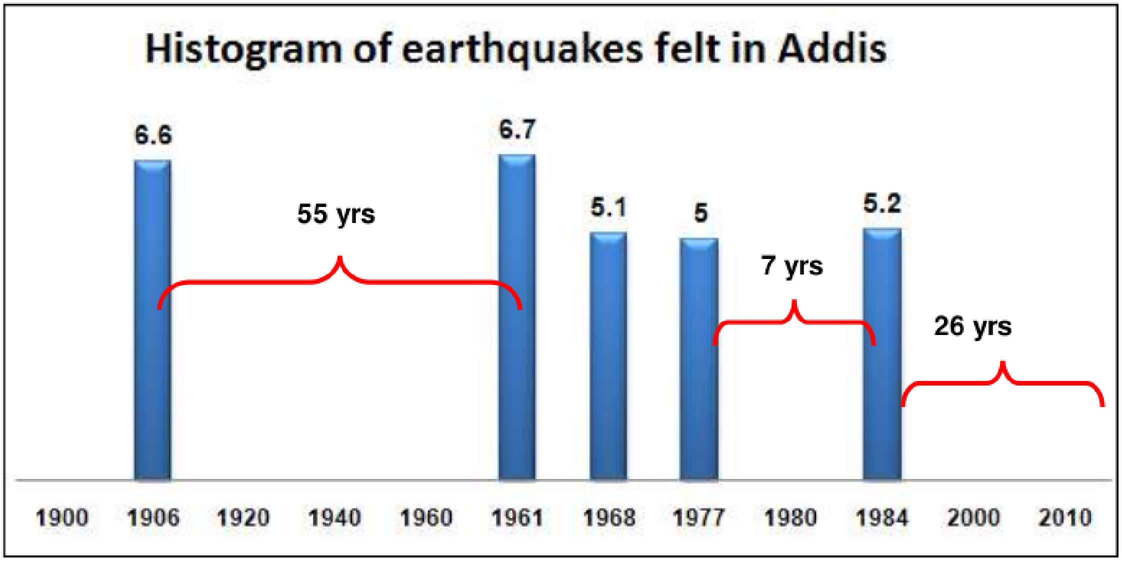

Figure 1.3 Histogram of major seismic events felt in Addis Ababa as reported by LM. Asfaw (1992) with time elapsed between major earthquake events. Note that there is no indication if the seismic events reported in M_L (local earthquake magnitude) or as M_S (surface wave magnitudes).

CHAPTER 2

THEORY OF SEISMIC WAVES

2.1 The seismic wave equation

Earthquakes and other disturbances generate seismic waves, which give information about the sources of the waves and the material they pass through. Seismic waves propagate through the earth because the material within it can undergo internal deformation.

The equation of motion has solutions that describe the two types of propagating seismic (elastic) waves. These are compression and shear waves.

The equation of motion

$\sigma_{ij,j}(x, t) + f_i(x, t) = \rho \frac{\partial^2 u_{i(x,t)}}{\partial t^2}$--------------------------- (2.1)

These wave types propagate differently, with velocities that depend in difference on the elastic properties of the material.

Let us consider a homogeneous region one of uniform properties of the material. We assume that the region contains no source of seismic waves, which require a body force. Once the waves propagate away from the source, the relation between the stresses and displacements is given by the homogeneous equation of motion, which includes no body force term, so F=ma becomes

$\sigma_{ij,j}(x, t) = \rho \frac{\partial^2 u_{i(x,t)}}{\partial t^2}$-------------------------------------(2.2)

Solving equation (2.2) in Cartesian (x, y, z) coordinate system, beginning with the x component

$\frac{\partial \sigma_{xx}(x,t)}{\partial x} + \frac{\partial \sigma_{xy}(x,t)}{\partial y} + \frac{\partial \sigma_{xz}(x,t)}{\partial z} = \rho \frac{\partial^2 u_x(x,t)}{\partial t^2}$------------- (2.3)

To express this in terms of displacements, we use constitutive law for an isotropic elastic medium,

$\sigma_{ij} = \lambda\theta^{\delta}{}_{ij} + 2\mu\sigma_{ij}$-------------------------------------- (2.4)

Writing the strain in terms of displacements, we get

σ_{xx}=λθ + 2μe_{xx} = λθ + 2μ$\frac{\partial u_x}{\partial x}$

σ_{xy}= 2μe_{xy} = μ ($\frac{\partial u_x}{\partial y}$ +$\frac{\partial u_y}{\partial x}$)

σ_{xz}= 2μe_{xz} = μ ($\frac{\partial u_x}{\partial z}$ +$\frac{\partial u_z}{\partial x}$) --------------------------- (2.5)

Next we take the derivatives of the stress components

$\frac{\sigma_{xx}}{\partial x}$= λ$\frac{\partial \theta}{\partial x}$ + 2μ$\frac{\partial^2 u_x}{\partial x^2}$

$\frac{\sigma_{xy}}{\partial y}$= 2μ ($\frac{\partial^2 u_x}{\partial y^2}$ +$\frac{\partial^2 u_y}{\partial x \partial y}$)

$\frac{\sigma_{xz}}{\partial z}$= 2μ ($\frac{\partial^2 u_x}{\partial z^2}$ +$\frac{\partial^2 u_z}{\partial x \partial z}$) -------------------------------------- (2.6)

For a homogeneous material, the elastic constants do not vary with positions. Substituting the derivatives into the equations of motion and using the definition of dilatation

Θ = $\nabla \cdot u$ = $\frac{\partial u_x}{\partial x}$ + $\frac{\partial u_y}{\partial y}$ +$\frac{\partial u_z}{\partial z}$-------------------------------- (2.7)

And of the Laplacian

$\nabla^2 u_x$=$\frac{\partial^2 u_x}{\partial x^2}$ + $\frac{\partial^2 u_x}{\partial y^2}$ + $\frac{\partial^2 u_x}{\partial z^2}$---------------------------- (2.8)

Gives

(λ +μ)$\frac{\partial \theta}{\partial x}$ + μ $\nabla^2(u_x)$ =ρ$\frac{\partial^2 u_x}{\partial t^2}$------------------------------- (2.9)

For the x component of the equation of motion (2)

Similar equation can be obtained for the y and z component of displacement. The three equations can be combined, using the Laplacian of the operator of the displacement field

$u\nabla^2$= ($\nabla^2 u_x$ +$\nabla^2 u_y$ +$\nabla^2 u_z$) ------------------------------- (2.10)

Into a single equation

$(\lambda + \mu)\nabla(\nabla \cdot u(x, t)) + \mu\nabla^2 u(x, t) = \rho \frac{\partial^2 u(x,t)}{\partial t^2}$ --------------------- (2.11)

This is the equation of motion for an isotropic elastic medium written totally in terms the displacement, with the dependence on position and time explicitly. Equation (11) can be written using vector identity

$\nabla^2 u = \nabla(\nabla \cdot u) - \nabla \times (\nabla \times u)$ ----------------------------------- (2.12)

To get

$(\lambda + 2\mu)\nabla(\nabla \cdot u(x, t)) - \mu\nabla \times (\nabla \times u(x,t)) = \rho \frac{\partial^2 u(x,t)}{\partial t^2}$--------- (2.13)

We express the displacement field in terms of two other functions, ϕ and ϒ, which are potentials

$u(x, t) = \nabla\phi(x,t) + \nabla \times \Upsilon(x, t)$ ---------------------- (2.14)

In this representation, the displacement is the sum of the gradient of a scalar potential, $\phi(x, t)$, and the curl of a vector potential, $\Upsilon(x, t)$, both of are function of space and time. Because the vector identity

$\nabla\phi = 0$ ------------------------- (2.15)

Separate the displacement field into two parts. The part associated with the scalar potential has no curl or rotation and gives rise to compressional waves. Conversely, the part associated with the vector potential has zero divergence, causes no volume change, and corresponds to shear waves. Because taking the curl discards any part of the vector potential that would give rise to a nonzero divergence, we require that the vector potential satisfy $\nabla \cdot \Upsilon(x, t) = 0$.Substituting the potential into (13) and rearranging terms using equation (15) yields.

$(\lambda + 2\mu)\nabla(\nabla^2\phi) - \mu\nabla \times \nabla \times \nabla \times \Upsilon = \rho \frac{\partial^2}{\partial t^2}(\nabla\phi + \nabla \times \mathbf{\Upsilon})$ -------------- (2.16)

Using equation (12), the second part of equation (16) simplifies to

$\nabla \times \nabla \times \nabla \times \mathbf{\Upsilon} = -\nabla^2(\nabla \times \mathbf{\Upsilon}) + \mathbf{\nabla}(\mathbf{\nabla}.(\mathbf{\nabla} \times \mathbf{\Upsilon})) = -\nabla^2(\nabla \times \mathbf{\Upsilon})$ -------- (2.17) because the divergence of the curl gives zero. After this substitution, the terms in equation (16) can be regrouped to give

$$\nabla\left[(\lambda+2\mu)\nabla^2\phi(x,t)-\rho\frac{\partial^2\phi(x,t)}{\partial t^2}\right]=-\nabla\times\left[\mu\nabla^2\phi(x,t)-\rho\frac{\partial^2\phi(x,t)}{\partial t^2}\right] \text{-------} \quad (2.18)$$

because the elastic constants do not vary with position, and the order of differentiation has no effect.

One solution of the equation can be found if both terms in the bracket are zero.

$$\nabla\left[(\lambda+2\mu)\nabla^2\phi(x,t)-\rho\frac{\partial^2\phi(x,t)}{\partial t^2}\right]=0 \text{-------------------------} \quad (2.19)$$

The scalar potential satisfies

$$\nabla^2\phi(x,t)=\frac{1}{\alpha^2}\frac{\partial^2\phi(x,t)}{\partial t^2} \text{--} \quad (2.20)$$

with velocity $\alpha=\left[\frac{(\lambda+2\mu)}{\rho}\right]^{\frac{1}{2}}$ -- (2.21)

this solution corresponds to P waves, or compression waves.

Similarly the vector potential satisfies

$$\nabla^2\Upsilon(x,t)=\frac{1}{\beta^2}\frac{\partial^2\Upsilon(x,t)}{\partial t^2} \text{---------------------------------------} \quad (2.22)$$

with velocity $\beta=\left(\frac{\mu}{\rho}\right)^{\frac{1}{2}}$ which corresponds to S, or shear waves.

Waves on a string satisfied the wave equation

$$\frac{\partial^2 u(x,t)}{\partial x^2}=\frac{1}{v^2}\frac{\partial^2 u(x,t)}{\partial t^2} \text{---} \quad (2.23)$$

Describes the propagation of a scalar quantity in one dimensional space. The scalar potential satisfies a similar scalar wave equation, with the difference that the space variable **x** is in three dimensions. The vector potential, a vector quantity, satisfies the analogues wave equation in three dimensions.

The wave equation 2.20 and 2.22 are strictly valid only for a homogeneous medium because they were derived with the assumption that all derivatives of the elastic constants were zero. The wave equations are valid for any coordinate system.

2.2 Plane waves

The scalar wave equation in three dimensions,

$\nabla^2\phi(x,t)= \frac{1}{v^2}\frac{\partial^2\phi(x,t)}{\partial t^2}$--- (2.24)

describes how the scalar field $\phi(x,t)$ propagates in three dimensions. It is a homogeneous wave equation, with no forcing function to act as a source of the waves. If there were, the inhomogeneous scalar wave equation in three dimensions with a source term *f(x, t).*

$\nabla^2\phi(x,t)- \frac{1}{v^2}\frac{\partial^2\phi(x,t)}{\partial t^2}$ = *f(x, t)* ------------------------------------ (2.25)

would apply.

The harmonic wave solution to the scalar wave equation in one dimension is

u(x, t) = A$e^{i(\omega t\pm kx)}$-- (2.26)

can be generalized to solve the tree dimensional scalar wave equation. This solution, known as harmonic plane wave, is written

$\phi(x,t)$ =Aexp (i (ωt$\pm$**k·x)) =** A exp (i(ωt$\pm k_x x \pm k_y y \pm k_z z$)----- (2.27)

Where x is the position vector, and **k = (**k_x, k_y, k_z) is now the wave vector, also called the wave number vector. This solution describes a plane wave propagating in an arbitrary direction given by the wave vector. To show this, we write k = $[k]\hat{k}$, where $\hat{k}$ is a unit vector along the direction of k; so Eqn (27) become

$\phi(x,t)$ =A exp (i(ωt$\pm|k|\hat{k}$ ·x)) -------------------------------- (2.28)

A plane wave propagating in the $\hat{k}$ direction with velocity

$v = {}^{\omega}/_{|k|}$--- (2.29)

Thus the wave vector describes two important features of a propagating wave. Its magnitude gives the wave number, the spatial frequency, and its direction gives the direction of propagation. The wave front, which at any time are surfaces of constant phase (ωt - k·x) and constant values of $\phi(x,t)$,are planes perpendicular to direction of propagation.

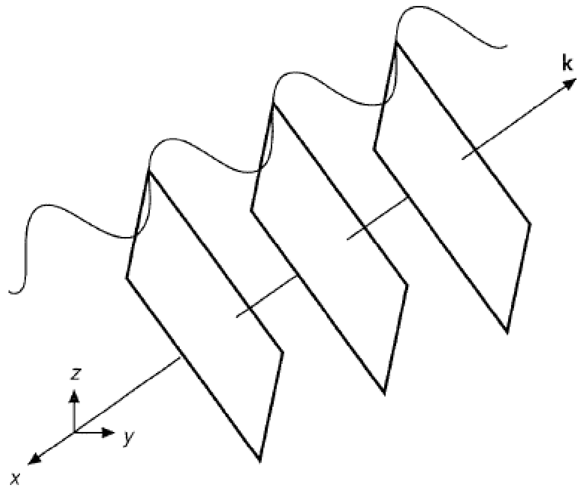

Fig. 2.1 Wave fronts for the harmonic plane wave traveling in the direction indicated by the wave vector. The wave length is λ= 2π/$|k|$ (Stein and Wysession, 2003)

Note that all points on a plane perpendicular to the wave vector have the same value of **k · x,** because this scalar product is the projection of **k** on **x.** The phase is periodic over a distance along the propagation direction equal to the wavelength, 2π/$|k|$

This solution to three dimensional scalar wave equation, can be generalized to solve the vector wave equation in three dimensions,

$\nabla^2 \Upsilon(x,t) = \frac{1}{v^2}\frac{\partial^2 \Upsilon(x,t)}{\partial t^2}$--- (2.30)

which describes the propagation of a vector field. In Cartesian coordinate, this break into three scalar wave equations

$\nabla^2 \Upsilon_x(x,t) = \frac{1}{v^2}\frac{\partial^2 \Upsilon_x(x,t)}{\partial t^2}$

$\nabla^2 \Upsilon_y(x,t) = \frac{1}{v^2}\frac{\partial^2 \Upsilon_y(x,t)}{\partial t^2}$

$\nabla^2 \Upsilon_z(x,t) = \frac{1}{v^2}\frac{\Upsilon_z(x,t)}{\partial t^2}$--------------------------------------- (2.31)

The harmonic plane wave solution to the vector wave equation is then

$u(x,t)$=**A** exp (i (ωt - k· x)) ------------------------------------ (2.32)

Here $\Upsilon(x,t)$ and the constant **A** are vectors**.**

2.3 Spherical waves

A second solution to the three-dimensional scalar wave equation yields waves with spherical, rather than planer wave fronts. To obtain this solution we express a scalar potential, $\phi(x,t)$ and its Laplacian in spherical coordinates.

$\nabla^2\phi(r,t) = \frac{1}{r^2}\frac{\partial}{\partial r}(r^2\frac{\partial\phi(r,t)}{\partial r}) + \frac{1}{r^2 sin\theta}\frac{\partial}{\partial\theta}(\sin\theta\frac{\partial\phi(r,t)}{\partial\theta}) + \frac{1}{r^2 sin^2\theta}\frac{\partial^2\phi(r,t)}{\partial\phi^2}$------ (2.33)

We consider spherically symmetric solutions where ϕ is a function of time and the radius r, so only the $\partial\phi$ /∂r term in the Laplacian survive. The spherically symmetric waves satisfy the homogenous wave equation.

$\nabla^2\phi(r,t) = \frac{1}{r^2}\frac{\partial}{\partial r}(r^2\frac{\partial\phi(r,t)}{\partial r}) = \frac{1}{v^2}\frac{\partial^2\phi(x,t)}{\partial t^2}$------------------------ (2.34)

where the space variable is the radius r rather than the position vector **r.** To solve this equation, we substitute

$\phi(r,t)$=ξ(r, t)/r --- (2.35)

And get

$\frac{1}{r}\left[\frac{\partial^2\xi}{\partial r^2} - \frac{1}{v^2}\frac{\partial^2\xi}{\partial t^2}\right]$= 0 --- (2.36)

Because the term in brackets is the scalar wave equation in one dimension, any function of the

$\xi = f(r \pm vt)$ satisfies Eqn 2.36 when $r \neq 0$. Thus any function of the form

$\phi(r,t) = f(r \pm vt)\ /r$ -- (2.37)

is spherically symmetric solution to the scalar wave equation.

This solution describes spherical wave fronts centered on the origin r = 0, whose amplitude depends the distance from the origin. When the minus sign is used on the above equation, it represents waves diverging outward from a source at the origin, with the amplitude decaying as 1/r.

However Eqn 37 is not a solution to the homogeneous equation everywhere in space, because it is infinite at r = 0. Physically this is because a wave spreading out from a point must have been generated by a seismic source there. Thus the outgoing wave $\phi(r,t)$ = f (t-r/v)/r, is actually a solution to the inhomogeneous wave equation

$\nabla^2\phi(r,t) - \frac{1}{v^2}\frac{\partial^2\phi(r,t)}{\partial t^2} = -4\pi\delta(r)\ f\ (t)$ ------------------------------ (2.38)

This represents a point source at the origin with a time function f(t). The delta function δ(r) is zero except at r=0, but its integral over a volume including the origin is 1. Thus integrating over a volume including the origin shows that Eqn 37 is a solution to the inhomogeneous scalar wave equation (38) even at the origin.

Spherical wave solution (Eqn 37) represents an ongoing wave generated at the origin explains the distant-dependent amplitude factor 1/r, which have no equivalent in the plane wave solution. As a spherical wave front, $4\pi r^2$, increases. The energy per unit area of the wave front transported by a propagating wave is proportional to the amplitude squared, the energy per unit wave front decays as $1/r^2$. This decay, called geometrical spreading conserves energy.

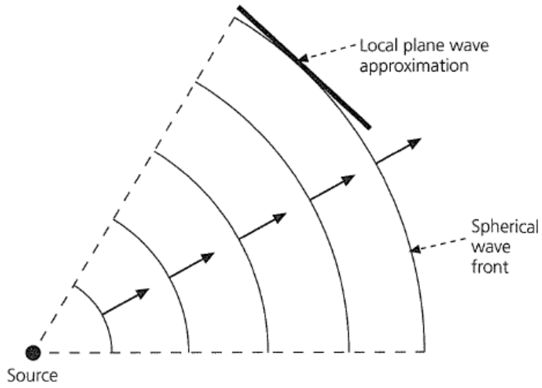

Figure 2.2. Spherical wave front spreading out from a source. The wave length is λ= 2π/$|k|$ (Stein and Wysession, 2003)

A plane wave front can be regarded as a limit of a spherical wave far from the source, because the spherical wave front becomes almost planar. This approximation is often used in seismology when seismometers are far from earthquakes.

2.4 P and S waves

We found earlier that the displacement can be separated into a scalar potential corresponding to P waves that satisfies the scalar wave equation.

$\nabla^2\phi(x,t)=\frac{1}{\alpha^2}\frac{\partial^2\phi(x,t)}{\partial t^2}$--- (2.39)

And a vector potential corresponding to S waves that satisfies the vector wave equation.

$\nabla^2\Upsilon(x,t)=\frac{1}{\beta^2}\frac{\partial^2\Upsilon(x,t)}{\partial t^2}$--- (2.40)

Let us consider a plane wave propagating in the z direction. The scalar potential for a harmonic plane P wave satisfying Eqn 39 is

Φ (z, t) = A exp (i(ωt – kz)) -----------------------------------(2.41)

So the resulting displacement is the gradient

u(z, t)= $\nabla\phi(z,t)$ =(0, 0, - kz) A exp (i(ωt – kz)) -------------(2.42)

Which has a non-zero component only along the propagation direction z. the corresponding dilatation is non-zero,

$\nabla \cdot u(z,t)$ =- k^2 A exp (i(ωt – kz)) ---------------------------(2.43)

Therefore, a volume change occurs. As the wave propagates, the displacements in the direction of propagation cause material to be alternatively compressed and expanded. Therefore, the P wave generated by the scalar potential is called compression wave.

On the other hand the S wave, or shear wave, described by the vector potential

$u(z,t)$= (A_x +A_y + A_z) exp (i(ω t – kz)), --------------------(2.44)

The resulting displacement fiend is given by the curl

u (z, t) = $\nabla \times \Upsilon(z,t)$ = (ikA_y, -ikA_x, 0) exp (i(ωt – k z)),----- (2.45)

Whose component along the propagation direction z is zero. Thus the displacement associated with a propagating shear wave is perpendicular to the direction of propagation. A shear wave causes no volume change, because the dilatation $\nabla \cdot u(z,t)$, is zero.

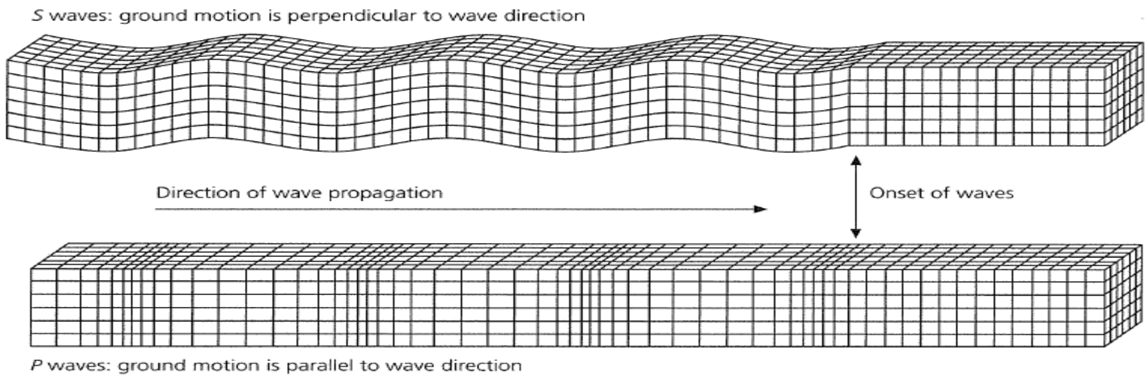

Fig 2.3Particles displacement produced by plane wave compression and shears waves, shown by a “snap shot” in time.

P waves produce displacement in the direction of wave propagation and volume change. S waves produce displacement perpendicular to the direction of wave propagation and distort the material without volume change.

A compression wave is an example of longitudinal waves, because the propagating displacement varies in the direction propagation. An example of longitudinal wave is a sound wave in air, which can be described as compression (elastic) wave in ideal fluid. On the other hand, a shear wave is an example of a transverse wave, because the propagating displacement field varies at right angle to the direction of propagation. Electromagnetic waves are another familiar example of transverse waves.

The component of Υ (z, t) in the direction of wave propagation (A_z) has no effect on the displacement field because taking the curl discards it. Only A_x and A_y contribute to the displacement. Because each component of the displacement depends on only one of these terms, there can be two independent shear wave fields. If A_x or A_y is zero, there will be only a *y* and *x* component of displacement. Thus, shear waves can have two independent polarizations, as is the case for other transverse waves, such as light.

In real applications, we define the z-axis as the vertical direction and orient the *x-z* plane along the great circle connecting a seismic source and a receiver. Plane waves travelling on the direct path between the source and receiver thus propagate in the *x-z* plane. The shear wave polarization directions are defined as SV, for shear waves with displacements in the vertical *x-z* plane, and SH for horizontally polarized shear waves with displacements in the *y* direction, parallel to the earth's surface. Both have displacements perpendicular to the propagation direction and the other polarization.

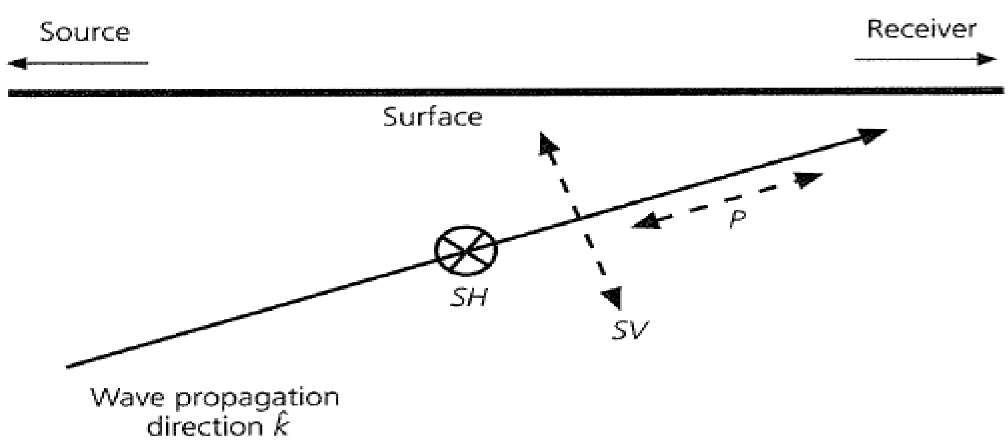

Fig 2.4 Displacement fields for plane P and S waves propagating in the x-z plane containing the source and receiver, where the z-axis is vertical. The P-wave displacement is along the wave vector *k*. The S wave can be decomposed into two polarizations, SV and SH, perpendicular to the wave vector (Stein and Wysession, 2003) .

P and SV waves are coupled with each other when they interact with horizontal boundaries, whereas SH remain separate.

Seismometers record the horizontal motions in the north-south and east-west directions, which rarely correspond exactly to the SH and SV polarizations. As a result, data from the horizontal components of seismometers are often *rotated*. The direction connecting the source and the receiver, corresponding to SV displacements, is called the *radial* direction, so a seismogram rotated to this direction is called the *radial* component. Similarly, the orthogonal component direction corresponding to SH displacement is called *transverse* direction, so a seismogram rotated to this direction is called the transverse component.

The definition of P wave velocity, termed as α and v_p,

$$\alpha = \left[\frac{\lambda+2\mu}{\rho}\right]^{1/2} = \left[\frac{K+4\mu/3}{\rho}\right]^{1/2} \text{-------------------------------------} \quad (2.47)$$

And S- wave velocity, terms β or v_s,

$$\beta = \sqrt{\frac{\mu}{\rho}} \text{---} \quad (2.48)$$

Shows that the seismic velocities depend in different ways on the elastic constants of the material. Because the rigidity μ and bulk modules K are positive, P waves travel faster than S waves. Thus, the first wave to arrive first arriving from an earthquake is always a compressional wave. As a result, the nomenclature P originally denoted the first arriving, “primary” wave, whereas S denoted the “secondary” wave.

Although both velocities depend on the rigidity, the shear velocity does not depend on the bulk modules K, because these waves involve no volume changes. Because the shear velocity is proportional to the square root of the rigidity, shear waves cannot propagate through the ideal (μ = 0) fluid. However, compressional waves propagate in ideal fluid with a velocity proportional to $K^{1/2}$. Thus, only compressional waves can travel through the earth’s outer core or the ocean.

The “seismic spectrum” showing the seismic waves of various frequencies and types in the following figure

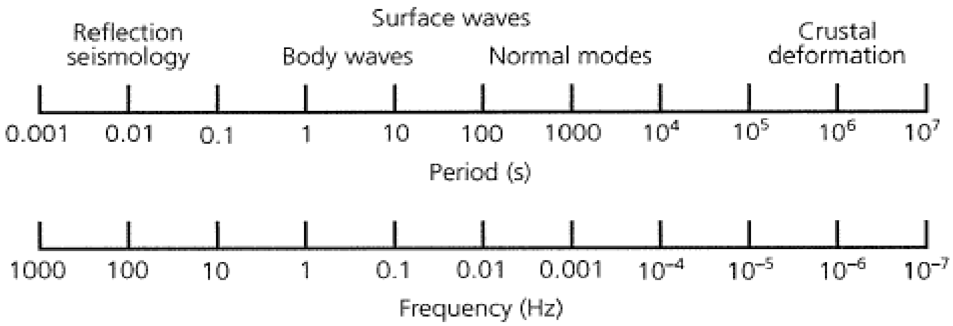

Fig 2.5 Seismic spectrum showing the frequencies at which varies analysis are conducted (Stien and Wysession, 2003)

Studies of earthquake typically use the period range from approximately 0.1s to more than 3000s, or frequencies from 10Hz to 0.0003Hz. Higher frequency waves of 20-80Hz generated by explosions or other artificial sources are used in the reflection seismology to explore the earth’s crust. Still higher frequencies 3−12 KHz, propagating primarily in the ocean, are used by marine geophysics to map the sea floor. At the other end of the spectrum, ground motions with periods longer than 10^4s are due to the crustal motions rather than propagating seismic waves.

CHAPTER 3

GEOLOGY AND TECTONIC SETTING

3.1 Geology of the area

The geology of Addis Ababa is characterized by different volcanic rocks with both acidic and basic compositions (Morton, 1976). The volcanic rocks are classified into Entoto trachyte, Intoto mixed rocks, Foota basalt, Cheleka basalt, Repi basalt (trachy basalt, basalt), lower ignimbrite, Quaternary olivine basalt, quaternary scoria, Teriary sediment and lake sediment. In addition, they are correlated with the volcanic rocks of central Ethiopia. In addition, the sedimentary rocks are Tertiary intravolcanic lake sediment. North of the city, the Oligocene plateau basalts (Ashangi and Aiba basalts) and the probably Miocene basaltic shield volcanoes (Termaber basalts) dominate the area. To the immediate north and bordering the northern part of the city on the Entoto hill chains silicic lavas and pyroclastics (Alaji rhyolites) of Miocene origin predominate. These are mainly rhyolites and trachytes. Welded tuff, volcanic breccia, tuffs and agglomerates make part of the sequence. Within the city, the so-called Basalts of Addis Ababa are wide spread together with the Younger Volcanics. The Younger Volcanics cover the whole region south, east and west of the city. The Basalts of Addis Ababa, Pliocene in age, are described as the youngest porphyritic olivine basalts, the intermediate age porphyritic feldspar basalts and the oldest aphanitic basalts. Of these basalts, the most diffuse is the olivine basalts (6.9 and 7.3 Ma). They cover a large area starting from just north Legahar up to the extreme north of the city to the foot of the Entoto hill. The less diffuse feldspar basalts (6.4 Ma) occupy a space covering from the central part of the city near the City Hall to the western most limit of the city to Burayo. The aphanitic basalts (3.6 Ma), on the other hand, extend from east to west of the city from Yeka to Gulele. They are also exposed at the southern parts of the city along the Bole International airport and following the rivers of Akaki and Kebena towards the Lideta Air Field. The Younger Volcanics (Pliocene–Pleistocene) constitute the youngest of all volcanic rocks in the Addis Ababa region. These are the silicic lavas and pyroclastics (Balchi rhyolites) and the olivine basalts (Bishoftu basalts). The Balchi rhyolites (3.5 and 3.2 Ma) include tuffs, ignimbrites, rhyolites and trachytes. They are exposed in the southern and eastern part of the city and beyond. The Bishoftu basalts (2.8 Ma) are exposed in the southeast direction from the city towards Akaki and Debrezeit (Bishoftu) towns.

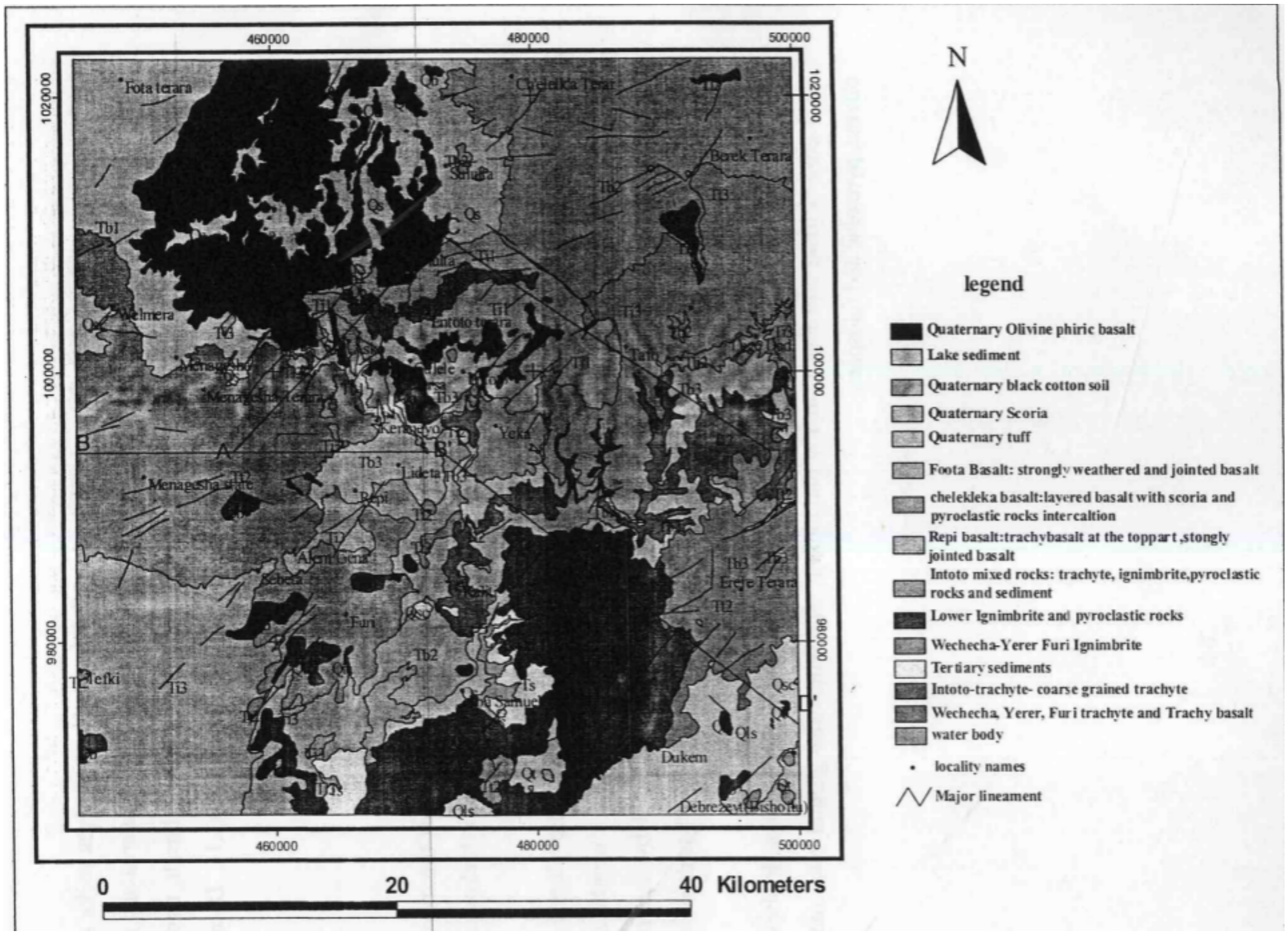

Figure 3.1 Geological map of Addis Ababa area adopted from Aseged Getahun (GSE, 2007)

3.2 Geological Structure

The area is highly tectonized and complex in structure because of its vicinity to the Main Ethiopian Rift (Getahun, 2007). Lineaments and faults are the main diastrophic structures, whereas the volcanic layering and its bedding are among the non-diastrophic structures that dominate the study area (Getahun, 2007).

3.2.1 Lineaments

Different geomorphic features align mostly to the NE-SW direction, which is parallel to the structure of the rift, or rift margin. Most of these lineaments are observed in all units as interpreted from digital elevation model and maximum length estimated is 5 Km (Getahun, 2007)

3.2.2 Fault

Most of the faults mainly observed in the SE part of the map area and cut the entire unit. They have a structure trending in NE-SW direction. These faults are mainly normal faults.

3.2.3 Joints and Fracture

The dominant structural trend of the joints followed the regional tectonic structural, i.e. Main Ethiopian rift tectonic trend. The lengths of the structures vary between few centimeters to several meters. In some places, they are oriented normal to the flow banding and parallel to each other (Getahun, 2007).

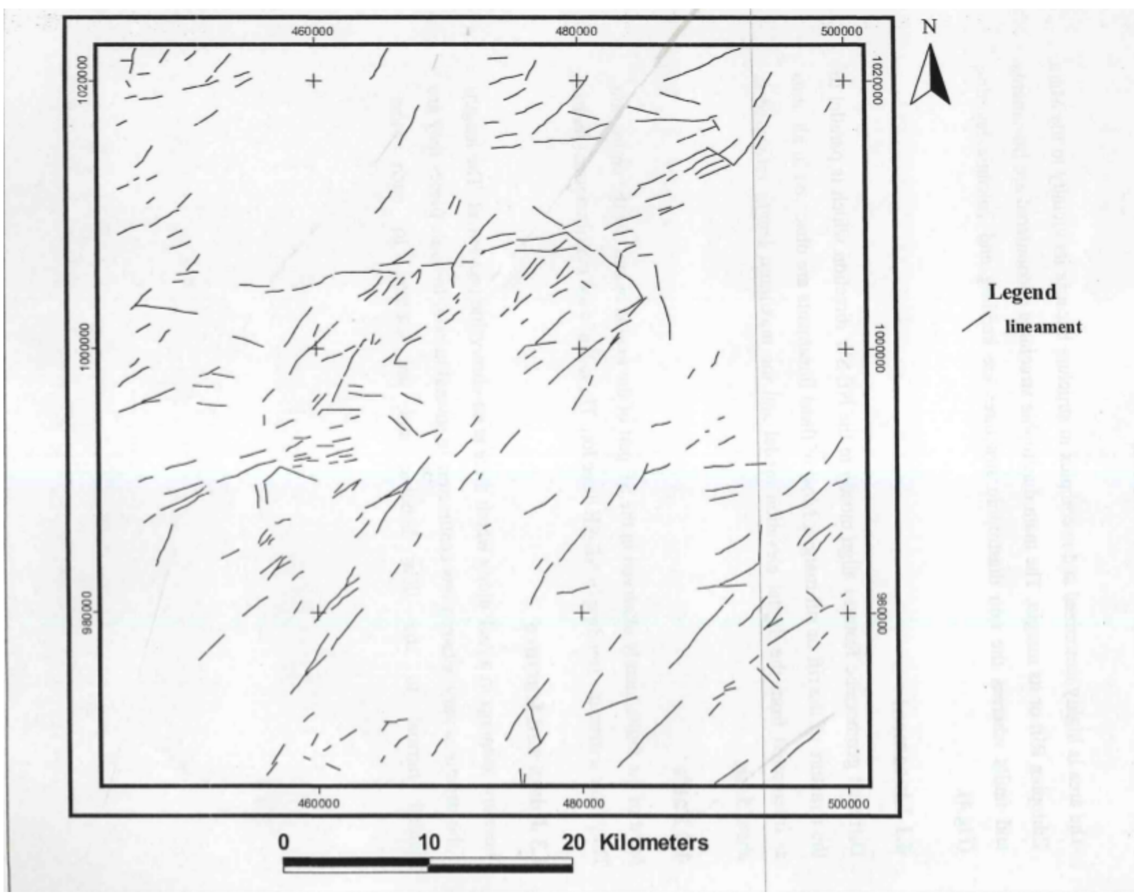

Figure 3.2 Structural map the study of the area, adopted from (Getahun, 2007).

CHAPTER 4

METHODOLOGY

4.1Earthquake Location

An iterative method of earthquake location proposed by Geiger (1912) is used in this study. For earthquake location, the velocity structure, which determined the ray paths and hence travels times, is crucial. Therefore, for this study crustal model made under EAGLE project (Keranen et al. 2004) on the study of crustal structure of Main Ethiopian rift is used.

The program Hypo2000 (Klein, 2002) used for seismic event location. These methods are based on linear zing the non-linear problem. The first step is to make guess of the hypo-center and origin time (x_0, y_0, z_0, t_0). Guess of the hypo-center and origin time done by using the location nearest station with the first arrival time and using that arrival time as t_0. In order to linearize the problem, it is now assumed that the true hypocentre is close enough to the guessed value so that travel-time residuals at the trial hypocentre are a linear function of the correction we have to make in hypocentral distance.

The calculated arrival times at station *i*, from the trial location are

$$t_i^{arr} = t_i^{tra}(x_i, y_i, z_i, x_o, y_o, z_o) + t_o = t_i^{tra} + t_o \text{------------} \quad (4.14)$$

Where $t_i^{tra}$is the calculated travel time as a function of the known station location (x_i, y_i, z_i), an assumed hypocenter location (x_o, y_o, z_o) and the velocity model t_0 the origin time of the event.

We now assume that the residuals are due to the error in the trial solution and the corrections needed to make them zero are Δx, Δy, Δz, and Δt. If the corrections are small, we can calculate the corresponding corrections in travel times by approximating the travel time function by a Taylor series and only using the first term.

Using standard least squares techniques and the corrections to the hypocenter and origin time is obtained. The original trial solution is then corrected and this new solution is used as trial solution for the next iteration. This iteration process can be continuing until a predefined breakpoint is reached. Breakpoint conditions can be either a minimum residual r, a last iteration giving a smaller hypocentral parameter changes than a predefined limit, or just the total number of iterations.

```
 date hrmn   sec      lat      long depth   no m    rms  damp erln erlt erdp
1612 7 1339 32.37  849.33N  38 55.8E  10.0    6 3  0.06 0.000  2.3  2.1  2.1
 stn   dist   azm  ain w phas    calcphs hrmn tsec  t-obs  t-cal    res   wt di
 FURI    29 286.4 98.3 0 P       PG      1339 38.1   5.74   5.74  -0.01 1.00*16
 FURI    29 286.4 98.3 0 S       SG      1339 42.3   9.94   9.93   0.00 1.00*33
 AAE     30 322.4 97.8 0 P       PG      1339 38.4   6.00   5.90   0.09 1.00*10
 AAE     30 322.4 97.8 0 S       SG      1339 42.5  10.16  10.21  -0.06 1.00*20
 AAE     30 322.4      0 IAML            1339 47.1   14.7
 AAE     30 322.4      0 IAML            1339 47.3   15.0
 WLRA    40 318.9 64.4 0 P       PN3     1339 40.0   7.64   7.72  -0.09 1.00*12
 WLRA    40 318.9 64.4 0 S       SN3     1339 45.8  13.42  13.36   0.05 1.00* 9

 AAE  BN   hdist:      31.3   amp:         298.0 T:   0.4   ml =   1.9
 AAE  BE   hdist:      31.3   amp:         212.1 T:   1.7   ml =   1.8
 2016 12 7 1339 32.4 L   8.822  38.931 10.0  IGS  3 0.1 1.9LIGS
 OLD: 12 7 1339 32.4 L   8.822  38.931 10.0  IGS  3 0.1 1.9LIGS
```

Figure 4.1 Example of the location of seismic events using four stations in SEISAN earthquake processing software

Alternatively, it can be written as

$d_i' = \mathrm{T}\,(x_i, x_o) + \mathrm{t}$ --- (4.15)

where, ***d****$_i$* *is the arrival time ,* ***T****(x_i, x_0)* travel time and **t** is the origin time

If the velocity structure is known, the forward problem is written as

d = A(**m**), or d_i = A(m_j)

It shows how the data vector (**d**), containing the arrival times at the stations, can be computed from an assumed model vector (**m**) composed of the source location and origin time,

m = (x, y, z, t**)** -- (4.16)

The inverse problem can be stated as; given the observed arrival times, find a model that fits them. To do this, we begin with a starting model m^o, which is an estimate of a model that we hope is the solution we need. The starting model predict that we would have observed data d_i^o = *A(m_j)*. This predicted data are not the same as the actually observed. Hence, we need changes Δm_j in the starting model

$m_j = m_j^o + \Delta m_j$-- (4.17)

That will make the predicted data closer to those observed. The data do not depend linearly on the model parameters, so we linearize the problem by expanding the in Taylor series about the starting modelm^o and keeping the linear term,

$d_i \approx d_i^o + \sum_j \frac{\partial d_i}{\partial m_j}\Big|_{m^o} \Delta m_j$---------------------------- (4.18)

Rearranging the above equation gives, difference between the observed data and those predicted,

$\Delta d_i^o = d_i' - d_i^o \approx \sum_j \frac{\partial d_i}{\partial m_j}\Big|_{m^o} \Delta m_j$ -------------------- (4.19)

Let us define the partial derivative matrix as

$G_{ij} = \frac{\partial d_i}{\partial m_j}$, -- (4.20)

So the equation becomes

$\Delta d = G\Delta m$, or $\Delta d_i = \sum_j G_{ij}\Delta m_j$--------------------- (4.21)

Eqn (4.21) is a vector- matrix equation representing a system of simultaneous linear equations. To solve it, we need a change in model Δmthat, when multiplied by known$G$, gives the required change in the dataΔd.

This an inverse problem, in contrast to the forward problem of finding the change in the data Δd predicted by the assumed change Δmin the model.

We generally have observations at many seismic stations, and are solving for four model parameters. In the notation above (Eqn 4.21), *j* ranges from 1 to 4, and *i* ranges from 1 to *n*, *n* is much greater than 4. Because each arrival time corresponds to one equation, and each model parameter provides one unknown, G has a number of rows equal to the number of arrival time observations, and a number of columns equal to the number of model parameters.

$$\begin{bmatrix} \Delta d_1 \\ \Delta d_1 \\ \cdot \\ \vdots \\ \vdots \\ \cdot \\ \Delta d_n \end{bmatrix} = \begin{bmatrix} G_{11} & G_{12} & G_{13} & G_{14} \\ G_{21} & G_{22} & G_{23} & G_{24} \\ \vdots & \vdots & \vdots & \vdots \\ G_{n1} & G_{n2} & G_{n3} & G_{n4} \end{bmatrix} \begin{bmatrix} \Delta m_1 \\ \Delta m_2 \\ \Delta m_3 \\ \Delta m_4 \end{bmatrix}$$ ------------------------- (4.22)

This over determined problem has its own difficulties. It is solved when n =4, the G become a 4$\times$ 4 square matrix, and then a solution is obtained by multiplying it by its inverse.

$G^{-1}\Delta d = G^{-1} G \Delta m = \Delta m$-- (4.23)

If the number of arrival time exceeds four, this method cannot be used, because G is not square thus does not have an inverse. We can use those four arrival times, discarding the rest of the data and get exact solution, but arrival times contain errors due to a variety of possible effects, including reading errors, inaccuracies in the clocks at the stations, and misidentification of the first arrivals. In addition to these errors, there are systematic errors because the velocity structure is not perfectly known and laterally variable. As a result, the equations are inconsistent: no one model can solve them exactly. The approach taken instead is to seek the origin time and source location that "best" solve the over-determined inconsistent equations.

We regard the observations d_i' as having errors described by their standard deviations σ_i and the model that minimizes the misfit,

$\chi^2 = \sum_i \frac{1}{\sigma^2}\left(\Delta d_i - \sum_j G_{ij}\,\Delta m_j\right)^2$---------------------------------- (4.24)

Which the prediction error, the normalized sum of the squares of the difference between the observed arrival times and those predicted by the model. χ^2, the fitting function to be minimized, weights the data by the reciprocal of their variances so that the most uncertain have the least effect. To find the best fit, we set partial derivatives of the misfit with respect to change in model parameters Δm_k equal to zero, and use the fact the model elements are independent, so the partial derivative of the change in one respect to those in others is zero,

$\frac{\partial \Delta m_j}{\partial \Delta m_k} = \delta_{jk}$-- (4.25)

The partial derivatives of the misfit are

$\frac{\partial \chi^2}{\partial \Delta m_k} = 0 = 2\sum_i \frac{1}{\sigma^2}\left(\Delta d_i - \sum_j G_{ij}\,\Delta m_j\right)G_{ik}$, ---------------------- (4.26)

or

$\sum_i \frac{1}{\sigma^2}\Delta d_i\, G_{ik} = \frac{1}{\sigma^2}\sum_i\left(\sum_j G_{ij}\,\Delta m_j\right)G_{ik}$, ---------------------------- (4.27)

If the variances of the data are equal ($\sigma_i^2 = \sigma^2$), that term can be factored out, and

$\sum_i \Delta d_i\, G_{ik} = \sum_i\left(\sum_j G_{ij}\,\Delta m_j\right)G_{ik}$----------------------------------- (4.28)

Or in matrix notation,

$G^T\Delta d = G^T G \Delta m$-- (4.29)

See that $\sum_i \Delta d_i\, G_{ik} = G^T\Delta d$

The advantage of this form is that although the matrix G cannot be inverted, the matrix G^TG is square and can be inverted. Eqn (4.29) thus gives Δm, the standard least squares solution to a set of equations that cannot be solved exactly, because

$\Delta m = (G^T G)^{-1} G^T \Delta d = G^{-g}\Delta d$, or $\Delta m_j = \sum_i G_{ji}^{-g}\,\Delta d_i$--------- (4.30)

The operator $(G^T G)^{-1}G^T$, which acts on the data to give the model, is called generalized inverse of G, and written as G^{-g}. it gives the best solution in the least square sense, because it gives the smallest squared misfit. The generalized inverse is analog of the inverse, but for a matrix that is not square and has an inverse, then G^{-1} = G^{-g}. If the data errors are not equal, the least square solution is weighted by the errors.

To use this method, we begin with a starting model with a guess of the hypocenter and the origin time (x_o, y_o, z_o, t_o) $m^o$and predicts the values expected for the data, d^o = A(m^o). We then form the residual vector giving the misfit to the data, Δd^o = $d' - d^o$, evaluate the matrix of partial derivatives about the starting model,

$G_{ij}=\frac{\partial d_i}{\partial m_j}\Big|_{m^o}$, -- (4.31)

and use the generalized inverse (Eqn 4.30) to find Δm^o, the change in the starting model that gives a better fit to the data. Thus a new model

$m^1 = m^o + \Delta m^o$--- (4.32)

Predicts the values of the data

d^1= A (m^1)

That should be closer to the observations than the predictions of the starting model. This can be tested by computing the difference between the observations and the predicted data for the new model Δd^1 =$d' - d^1$, and examining the total misfit $\sum(d_i^1)^2$ =$\sum(d_i' - d_i^1)^2$. This should be less than the corresponding misfit for the starting model$\sum(d_i^o)^2$. The total squared misfit is more useful than the total misfit is$\sum \Delta d_i$, because the latter could be small for large misfits of opposite signs.

Remember that the G matrix of partial derivatives was found by expanding the function that predicts the data (travel times) about the starting model in a Taylor series, and taking the linear terms. This expansion works well if the starting model is "close" to the actual model. If this is not the case, the linear approximation may not be a good one.

As a result, the method can be iterated. Once the model has been changed, a new partial derivative matrix

$G_{ij}=\frac{\partial d_i}{\partial m_j}\Big|_{m^1}$ is found by expanding the function that predicts the data about the *new* model. The generalized inverse method is then used to solveΔd^1= GΔm^1.

For further change in the model, Δm^1 that reduces the remaining misfit. This process is repeated until successive iterations produce only small changes in the model, and hence in the total misfit to the data.

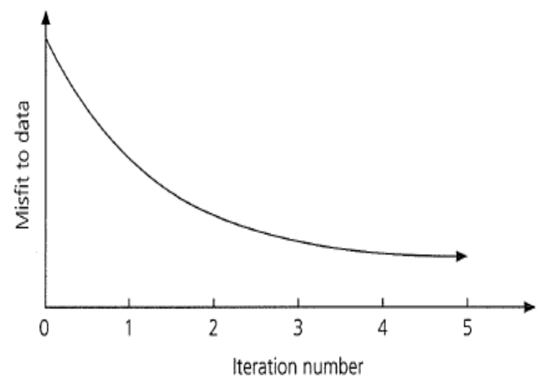

Figure 4.2 Schematic illustration of the variation in misfit to the data as a function of iteration number for an inverse problem (Stein and Wysession ,2003).

The following example show locating an earthquake with 10 stations, assuming a constant velocity model (Stein and Wysession, 2003). The stations are from 11 to 50 km from the hypo-center.

	Hypocenter	Start	1. Iteration	2. Iteration
X(km)	0.0	3.0	- 0.5	0.0
Y (km)	0.0	4.0	- 0.6	0.0
Z (km)	10.0	20.0	10.1	10.0
$t_o(s)$	0.0	2.0	0.2	0.0
e (s^2)		92.4	0.6	0.0
RMS (s)		3.0	0.24	0.0

Table 4.1 an example of inversion of error free data. Hypo-center is the correct location, Start is the starting location, and the location is shown for the two following iterations. Units for *x*, *y a*nd *z* are km, for t_o s and for the misfit *e*, it is s^2 (Haksov, 2010).

For this study seismic event location is made by using crustal model made by Keranen,et.al. and EAGLE working group(2002) on the study of crustal structure of Main Ethiopian rift under EAGLE (Ethiopia Afar Geo-scientific Lithospheric Experiment) project.

4.2 Errors in earthquake location

Because earthquakes are located using the arrival time data that have errors, the resulting locations and origin times have uncertainties. We characterize the errors in the data at the i^{th}station, d_i, by viewing the specific values measured as samples from a parent distribution that includes all possibled_i^k. The notation, d_i^k is the k^{th} sample ford_i, the arrival time at station *i*. For a large number of measurements (samples) from this distribution, the mean is the average

$$\bar{d}_i = \lim_{K\to\infty} \frac{1}{K}\sum_{k=1}^{K} d_i^{(k)}, \quad = \text{---}4.23$$

and the "spread" of the measurements is the variance

$$\sigma_i^2 = \lim_{K\to\infty}\left(\frac{1}{K}\sum_{k=1}^{K}(d_i^{(k)} - \bar{d}_i)^2\right). = \text{-------------------------- } 4.24$$

If the Gaussian parent distribution is an appropriate choice, there is a 68% probability that any sample will fall in the range $\acute{d}_i \pm \sigma_i$ and a 95% probability that any sample will fall in the range $\acute{d}_i \pm 2\sigma_i$.

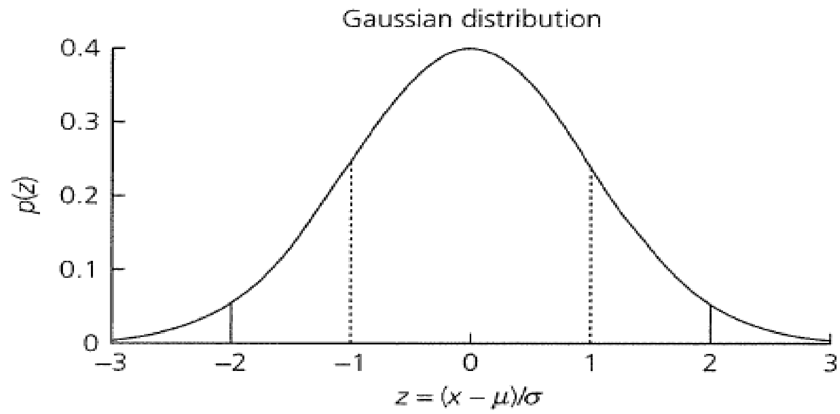

Figure 4.3 Probability density functions for a Gaussian distribution with mean μ and standard

deviation σ. The errors at different stations are described by the variance – covariance matrix of data

$\sigma_d^2 = \sigma_{d_j}^2$ =----------------------4.25

The diagonal (*i* = *j*) terms are the variances for data at individual stations. The off-diagonal terms

(*i* $\neq$ *j*) are the covariance that describe the relation between errors at pairs of stations. If the errors are uncorrelated between two stations for example, those due to station clock then how a measurement at one station differs from the mean there is unrelated to what occurs at another station, so their covariance is ideally zero. Given a finite number of real data, we expect the covariance to be small. By contrast, if the errors are correlated (for example, if one person was reading seismograms from different stations with a consistent bias), then similar deviations from the mean occur between these stations, and their co-variances would be larger . Errors can also be anti-correlated, such that deviations at a station tend to occur in one direction, whereas those at another station tend the other way, yielding negative covariance. Although errors of measurement are likely to be uncorrelated, systematic errors are often correlated.

The data are inverted using the generalized inverse solutions

$m_j = \sum_i G_{ji}^{-g} d_i$---4.26

As a result error in the model parameter can reflect errors in *all* of the data. Thus even if the errors in the data are uncorrelated; the resulting uncertainties in model parameters can be correlated. To see this, we write the co-variances of the model parameters in terms of those for the data.

$$\sigma_m^2 = \sigma_{m_{ij}}^2 = \lim_{K\to\infty} \frac{1}{K}\sum_{k=1}^{K}(m_j^{(k)} - \bar{m}_j)(m_i^{(k)} - \bar{m}_i) \quad \text{----------------------}4.27$$

$$\lim_{K\to\infty} \frac{1}{K}\sum_{k=1}^{K}\left(\sum_p G_{jp}^{-g}(d_p^{(k)} - \bar{d}_p)\right)\left(\sum_s G_{is}^{-g}(d_s^{(k)} - \bar{d}_s)\right)$$

$$\sum_p G_{jp}^{-g} \sum_s G_{is}^{-g}\left(\lim_{K\to\infty} \frac{1}{K}\sum_{k=1}^{K}(d_p^{(k)} - \bar{d}_p)(d_s^{(k)} - \bar{d}_s)\right)$$

$$= \sum_p G_{jp}^{-g} \sum_s G_{is}^{-g} \sigma_{d_{ps}}^2 \quad \text{---}4.28$$

This relation can be written in matrix form in terms of σ_d^2 andσ_m^2, the variance – covariance matrices for the data and model:

$$\sigma_m^2 = G^{-g}\sigma_d^2 G^{-g^T} \text{-------------------------------------}4.29$$

We often assume that the data are uncorrelated and equal, so that the data variance –covariance matrix is a constant times the identity matrix,

$$\sigma_d^2 = \sigma^2\delta_{ij}, \text{--}4.30$$

And the module variance - covariance matrix is

$$\sigma_m^2 = \sigma^2 (G^T G)^{-1} \quad \text{--------------------}4.31$$

The following table is an example of earthquake location with errors. In this case, Gaussian errors with mean zero and standard deviation 0.1s were added to the arrival times. The data are inconsistent and cannot fit exactly by any model. The inversion thus changes the model until a good, but not perfect, fit to the data is achieved. This final model, which is no longer changing much after three iterations, is close to, but not exactly, the model used to generate the data.

Invert for location and origin time

model evolution

parameter	actual value	model for iteration number 0	1	2	3
x	0.0	3.0	−0.2	0.2	0.2
y	0.0	4.0	−0.9	−0.4	−0.4
z	10.0	20.0	12.2	12.2	12.2
origin time	0.0	2.0	0.0	−0.2	−0.2

station location		residual for iteration number 0	1	2	3
35.0	9.0	−2.0	−0.1	0.1	0.1
−44.0	10.0	−3.0	−0.1	0.0	0.0
−11.0	−25.0	−3.8	0.0	0.1	0.1
23.0	−39.0	−3.2	−0.1	0.0	0.0
42.0	−27.0	−2.8	−0.2	−0.1	−0.1
−12.0	50.0	−2.1	−0.3	−0.1	−0.1
−45.0	16.0	−2.9	−0.1	0.0	0.0
5.0	−19.0	−3.7	−0.1	0.0	0.0
−1.0	−11.0	−4.0	−0.1	0.0	0.0
20.0	11.0	−2.5	−0.3	0.0	0.0
error		93.74	0.33	0.04	0.04

data standard deviation 0.10

model variance−covariance matrix

0.06	0.01	0.01	0.00
0.01	0.08	−0.13	0.01
0.01	−0.13	1.16	−0.08
0.00	0.01	−0.08	0.01

model standard deviation

x	*y*	*z*	origin time
0.25	0.28	1.08	0.10

Table 4.2 Earthquake location example with errors (Stein& Wysession, 2003)

The errors in the hypocenter and origin time can formally be defined with the variance – covariance matrix σ_m^2 of the hypo-central parameters. This matrix is defined as

$$\sigma_m^2 = \begin{bmatrix} \sigma_{xx}^2 & \sigma_{xy}^2\sigma_{xz}^2 & \sigma_{xt}^2 \\ \sigma_{yx}^2 & \sigma_{yy}^2\sigma_{yz}^2 & \sigma_{yt}^2 \\ \sigma_{zx}^2 & \sigma_{zy}^2\sigma_{zz}^2 & zt \\ \sigma_{tx}^2 & \sigma_{ty}^2\sigma_{tz}^2 & \sigma_{tt}^2 \end{bmatrix} \qquad (4.23)$$

To see that the results seem reasonable, we compare the final inversion model, taking into account its uncertainty, to the true model. The standard deviations of each parameter are given by the square root of the diagonal terms of the model variance- covariance matrix, so the final model (x =

0.2± 0.25km, y = −0.4±0.28km, z = 12.2 ±1.08km, t = − 0.2±0.10s) is an acceptable representation of the true model.

The variance of the depth estimateσ_{zz}^2, is larger than the corresponding terms σ_{xx}^2 andσ_{yy}^2 indicating that the depth is well constrained than the epicenter. This arises because of all the seismometers are at the surface, which is analogous to GPS. In some cases when the depth is poorly constrained, it is regarded as fixed, and only the epicenter and the origin time inverted for.

The uncertainties in the model parameter estimates are correlated, because the off-diagonal elements of the model variance-covariance matrix are nonzero. σ_{zt}^2 , the covariance of the depth and origin time uncertainties, is negative, indicating a trade-off between the focal depth and the origin time. At any station, similar arrival times result if the earthquake occurred earlier (t smaller) but deeper (z larger). Similarly,σ_{xy}^2, the covariance of the x and y location uncertainties in these two parameters are correlated. A method often used to illustrate this is to extract the 2× 2 sub-matrix

$$\begin{bmatrix} \sigma_{xx}^2 & \sigma_{xy}^2 \\ \sigma_{yx}^2 & \sigma_{yy}^2 \end{bmatrix}$$

and diagonalizable it by finding the eigenvalues λ^1 and λ^2, and the associated eigenvectors ($x_1^{(1)}$, $x_2^{(1)}$) and $x_1^{(2)}$, $x_2^{(2)}$). The uncertainties in the epicenter can then be thought of as an ellipse with semi-major and semi-minor axis $\lambda^{(1)1/2}$ and $\lambda^{(2)1/2}$, oriented in a given direction given by). An interesting feature of the error ellipse is that its shape and orientation depend on the $(G^T G)^{-1}$matrix, whereas the variance of the data, σ_d^2 , control the size of the ellipse. Because the shape of error ellipse depend on the geometry of the receivers it can examined without the reference to the specific data. As written, the ellipse is for confidence level of 1σ(68%), but ellipses are sometimes also given for 2σ(95%).

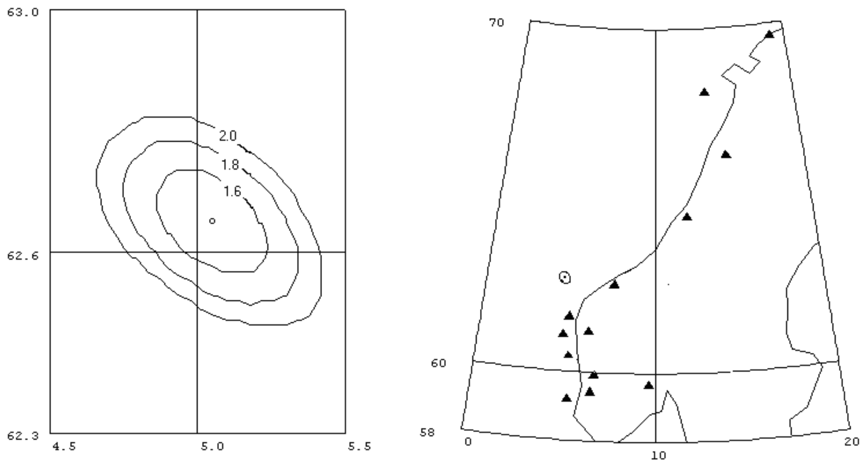

Figure 4.4 Left: RMS contours (in seconds) from a grid search location of an earthquake off western Norway (left).The grid size is 2 km. The circle in the middle indicates the point with the lowest RMS (1.4 s). Right: The location of the earthquake and the stations used. Note the elongated geometry of the station distribution (Havskov, 2010).

The *RMS* of the final solution is very often used as a criterion for “goodness of fit”. Although it can be an indication, *RMS* depends on the number of stations and does not in itself give any indication of errors (Stein and Wysession, 2003). Contouring the grid search RMS (Figure 4.6) gives an indication of the uncertainty of the epicenter. The question is now how to quantify this measure.

We can calculate contours within which there is a 67 % probability of finding the epicenter. We call this the error ellipse. This is the way hypocenter errors normally are represented. It is not sufficient to give one number for the hypocenter error since it varies spatially. Standard catalogs from PDE and ISC give the errors in latitude, longitude and depth; however, that can also be misleading unless the error ellipse has the minor and major axis NS or EW.

If we have no arrival time errors, there are no epicenter errors so the magnitude of the error (size of error ellipse) must be related to the arrival time uncertainties. If we assume that all arrival time reading errors are equal, only the size and not the shape of the error ellipse can be affected. Fig. 4.6 is an example of an elongated network with the epicenter off to one side. It is clear that in the NE direction, there is a good control of the epicenter since S-P times control the distances in this direction due to the elongation of the network. In the NW direction, the control is poor because of the small aperture of the network in this direction. We would therefore expect an error ellipse with the major axis NW as observed. Note, that if back azimuth observations were available for any of the stations far north or south of the event, this would drastically reduce the error estimate in the NW direction

4.3 Magnitude Calculation

The best way to quantify an earthquake is to calculate its magnitude. It is a number that characterizes the relative size or amount of elastic energy released by such a seismic event. There are several different magnitude scales in use and, depending on the network and distance to the event, one or several may be used (Lay & Wallace, 1995).

According to Lay and Wallace (1995) due to local variation in attenuation and ground motion, site amplification as well as of the station position with respect to the source radiation pattern, large variations in the measured amplitudes might occur, leading to large variance in magnitude estimates at individual stations.

According to Havsckov and Ottemðller(2010)magnitudes of earthquakes are calculated with the objectives to:

• Express energy release to estimate the potential damage after an earthquake.
• Express physical size of the earthquake.
• Predict ground motion and seismic hazard.

Amplitude and Period Measurements

Several magnitude scales use the maximum amplitude and often the corresponding period.
There are two ways of measuring this
(a) Read the amplitude from the base line and the period from two peaks. or
(b) Read the maximum peak-to-adjacent-trough amplitude and divide by 2. This is the most common and IASPEI (2005) recommended practice. It is also the simplest to do both manually and automatically. The period read either from two peaks or as half the period from the two extremes. This method will also to some extent average out large variation in the amplitude since it is not certain that one large swing is representative for the maximum amplitude. The peak-to-peak method will generally result in a smaller value than the zero to peak. Most display programs will automatically display the maximum amplitude zero to peak and for simplicity, unless otherwise noted.

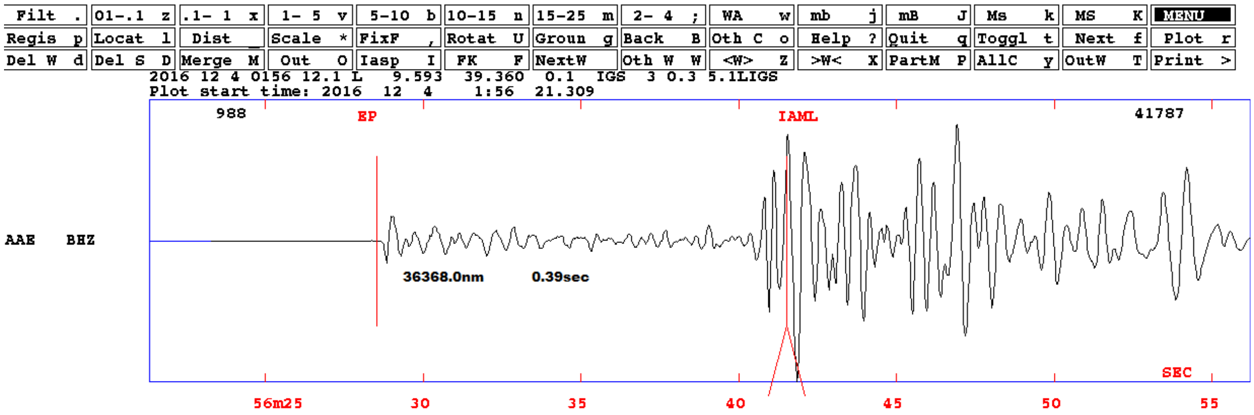

Figure 4.5 Reading amplitudes A from the base line and the period T from two peaks and calculating local magnitude in SEISAN software.

4.3.1 Local Magnitude M L

Richter (1935) defined the first magnitude scale for Southern California. All other magnitude scales are related to this scale. The local magnitude M_L is defined as

M_L = Log (A) + Q d (Δ) (4.25)

Where A is the maximum amplitude on a Wood-Anderson seismogram (which measures displacement for f > 2 Hz), Q d (Δ) is a distance correction function and Δ is epi-central distance. It was originally assumed that the gain of the Wood-Anderson seismograph was 2,800. However, it is now recognized that the most likely gain is 2,080 ± 60 (Uhrhammer and Collins, 1990). The original short period (SP) Wood-Anderson seismograph (damping 0.8 and natural frequency 1.25 Hz) measured displacement linearly above about 2 Hz and the maximum amplitude was measured as some kind of average of the amplitudes on the two horizontal components. In order to anchor the scale to some particular number, a magnitude 3 earthquake at 100 km distance was defined to have maximum amplitude of 1 mm on the seismogram.

While, horizontal components should be used to measure the amplitude, the practice is often to use the vertical component. Experience has shown that on a rock site, the maximum amplitudes on vertical and horizontal components are similar (e.g. Alsaker et al., 1991; Bindi et al., 2005), although there can be small differences (e.g. Siddiqqi and Atkinson, 2002). On soil, horizontal amplitudes are significantly higher than vertical amplitudes due to soil amplification. Thus using the vertical component instead of the horizontal components will give more consistent estimates of M_L among stations located on different ground conditions (Havskov & ottemoller, 2010).

Alternatively, station corrections can be used to compensate for the site conditions when using horizontal components.

For a local earthquake, the S-wave amplitude A as a function of hypocentral distance **r** can be expressed as

$A(r) = A_0\, r^{-\beta} e^{\frac{-\pi f r}{vQ}}$ (2.26)

where A_0 is the initial amplitude at distance 1, β is the geometrical spreading (1 for body waves and 0.5 for surface waves), f is the frequency, **v** the S-wave velocity and Q the quality factor inversely proportional to the an-elastic attenuation. Taking the logarithm gives

$\mathrm{Log}(A(r)) = -\beta \log(r) - 0.43\frac{\pi f r}{vQ} + \log(A_0)$ (2.27)

the distance attenuation term I

$Q_d(\Delta) = -\beta \log(r) - 2.3\frac{\pi f r}{vQ}$ (2.28)

Assuming a constant f, the M L scale can then be written as

$M_L = \mathrm{Log}\,(A) + a \log(r) + br + c$ (2.29)

where a, b and c are constants representing geometrical spreading, attenuation and the base level respectively. The parameters a, b and c can be expected to have regional variation and should ideally be adjusted to the local conditions.

Local magnitude M_L for events used to calculate magnitude less than 6–7 and distances less than 1,500 km with frequency band 1–20 Hz.

Local magnitudes (ML) of the earthquakes were computed from the maximum zero-to-peak amplitude measured on simulated Wood–Anderson displacement seismograms after removal of instrument response (Richter, 1935)

The parameters such as attenuation coefficients and correction factors for this study area used are those calculated for Ethiopia from study made by Keir (2006).

$M_L = \mathrm{Log}\,(A) + 1.20\,\mathrm{Log}(r) + 0.00107\, r - 2.17$ (2.30)

4.4 Discrimination between quarry blasts and earthquakes

Identification of the nature of a seismic source on the basis of its seismic signals that is, making a determination from seismographs as to whether it could be a nuclear explosion, or a natural earthquake, or a mine blast, Richards (1988), OTA (1988), Dahlman et al. (2009), and Bowers & Selby (2009).

Seismic methods for discriminating between earthquakes and explosions are based on interpretation of the event location, on the relative excitation of a variety of body waves and surface waves; and on properties of the signal spectrum associated with each of these two different types of sources (Richards, 1988).

Quarry explosion seismic events pose difficulty to seismic stations trying to catalog earthquake events, since they could be mistaken as local earthquakes.

Seismic monitoring of earthquakes and explosions

Here are the steps for earthquake and explosion monitoring; beginning with detection of signals and association of different signals to the same event. The next steps involve making a location estimate and identification.

Detection of seismic events

For detection, seismic monitoring is done with arrays of sensors, deployed around the city spread out over an area about 10 km 20km across (or less), that facilitate methods to enhance signal-to-noise ratios(Richards & Zhongliang, 2011). This is done typically by stacking signals from independent seismic sensors, often with appropriate delays to increase signal strength and reduce noise. By looking at the back azimuth of the event, we can also give estimates of the direction from which signals are arriving.

Practically, however, one of the often-cited expressions of monitoring capability is the magnitude threshold, above which 90% of the seismic events can be detected at more than three stations, the least number of stations for routine location (Havskov & Ottemoller, 2010).

4.4.1 Discrimination between quarry blasts and earthquakes using their spatial and temporal distribution.

Discrimination using spatial distribution focal depth (always at or near the surface for explosions and always below 5 km for micro-earthquakes), structure of the focal area (mostly sediments with low seismic velocities for explosions and block structures with substantially higher seismic velocities for micro-earthquakes) (Musil and Pleginger, 1996).

Explosion events are concentrated near the city following the distribution of quarry sites and most of epicenters of explosions are within radius of 30Km from the city center. Whereas earthquakes can originate from wide area following the trend of MER. Therefore, events registered beyond 30km can be exclusively classified as earthquakes. The seismic events within 30km from the city and with origin in the day time could be either earthquakes or explosion events.

Discrimination using temporal distribution

Almost all of origin time of events from quarry explosions are from 8:00Am to 5:00 PM in the day time, whereas natural earthquakes can happen at any time of the day, unlike explosions. Therefore any seismic event originating except between 8:00AM to 5:00PM can be classified as natural earthquakes .

Spectral method of discrimination of explosion and earthquake seismic events

The seismic waves that propagated from the source to seismic station are influenced by three factors: the first is the properties of the source and the second is the structure in the vicinity of the source and between the source and stations, while the third is the recording conditions at the station. It is not simple to study the properties of the seismic source independently of the other factors, especially if the structure in the source region and between the source and seismograms receivers is not known (Walter et.al, 1995). It is clear that, the mechanism the natural earthquakes are rather different from the mechanism of explosions. So, the seismic waves propagated from natural earthquakes and explosions considerably influenced the generation mechanism (Hussein, 1994).

Waveform and Mechanism of explosions and natural earthquakes

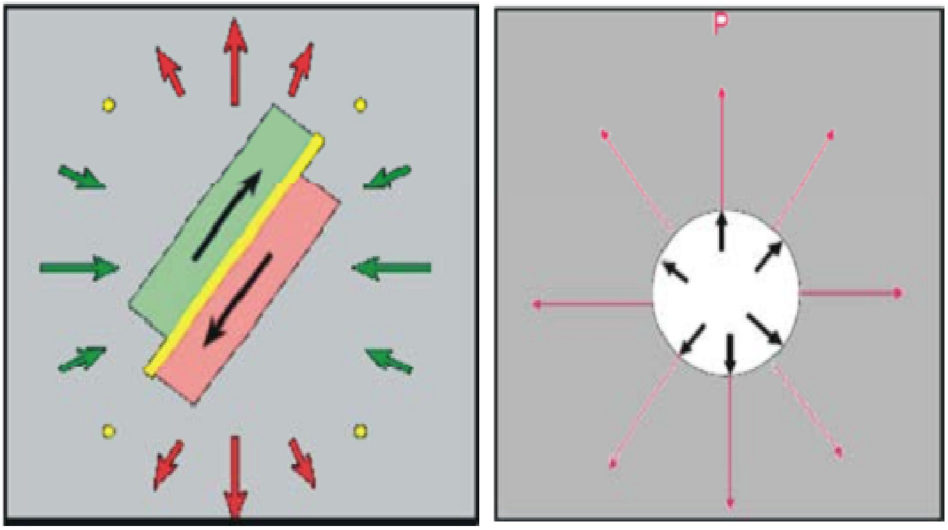

Fig. 4.6: Seismic source mechanism for natural earthquakes and explosions (Dahy & Abdrabou, 2012)

The mechanism for propagation of seismic energy is spherically symmetrical radiating longitudinal waves of equal magnitude in all direction. This is the theoretical assumption, this do not happen in reality because of the inhomogeneous nature of the Earth's crust. Therefore, explosions lack symmetrical radiation and generate transverse waves even though not expected theoretically. According to Hussein (Hussein, 1994), for any earthquake, the double couple character with quadric-polar radiation pattern of the generated P-waves depends upon the fault geometry and ray direction (for both body and surface waves).Source properties (predominantly volumetric changes for explosions and predominantly non-isotropic radiation for micro-earthquakes) (Musil & Pleginger, 1996).

Seismic events generate many different types of seismic wave, in various different frequency bands as shown in Figure 4.7 and different types of seismic source generate a different mix of seismic waves.

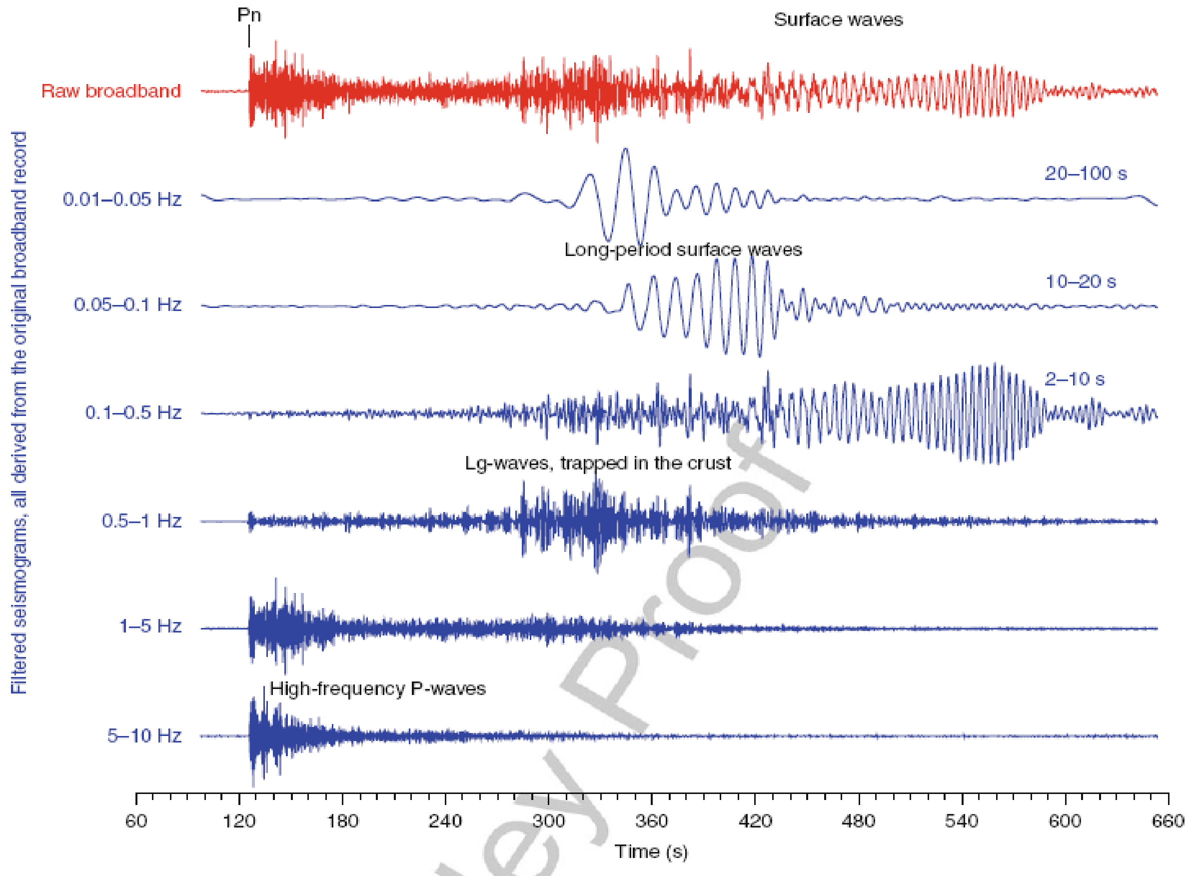

Figure 4.7 Seismic Monitoring of Nuclear Explosions. The seismograph recorded at station WMQ in northwestern China, for an underground nuclear explosion on July 8, 1989 in Kazakhstan at a distance of almost 1,000 km, is shown in red (top). Filtered versions of the original trace in different frequency bands are shown in blue. (Adapted from W.-Y .kim.)

A variety of waveform-based discrimination methods have been developed and investigated over the last five decades (see Stump et al., 2002 for a recent review). These methods can be roughly divided into: (i) determining amplitude ratios between seismic phases (e.g., Bennett and Murphy, 1986; Wuester, 1993; Plafcan et al., 1997; McLaughlin et al., 2004), (ii) spectral methods (e.g., Taylor et al., 1988; Gitterman and van Eck, 1993; Smith, 1993; Wal-ter et al., 1995; Carr and Garbin, 1998; Gitterman et al., 1998; Hedlin, 1998), and (iii) coda studies (e.g., Su et al., 1991; Hartse et al., 1995).

Body and Surface Wave Amplitudes ratio (Ap/As) Method:

Many studies on discrimination between quarry blasts and natural earthquakes at local or regional distances during the last decade have been based on variations of spectral characteristics of direct wave phases like (Pn, Pg, Lg, Rg, etc.) or on spectral ratios at different frequencies. Blasts and earthquakes have yielded different spectral amplitudes for the same direct wave phase at regional distances in many instances (Smith, 1989.), which can be used discriminate underground explosions from earthquakes.

Underground explosions like quarry explosions generate signals, which tend to have surface or S-wave amplitude (As) and body amplitude (Ap) that differ from those of natural earthquake signals. This is basically a result of explosions emitting more energy in the form of body waves (high-frequency seismic radiation) and earthquakes emitting more energy in the form of surface waves (low- frequency seismic radiation).The underlying idea for this comparison is the preferential excitation of P energy relative to S energy for explosive source. To use this method, both Ap and As values (maximum trace amplitude of P and S-waves in m) are required in this study.

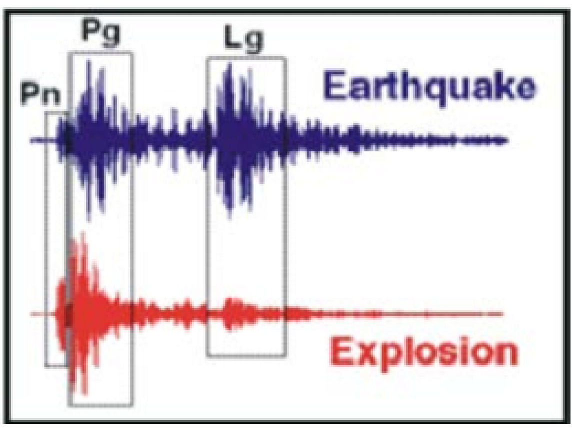

Figure 4.8 Example of earthquake and explosion seismograms (*Dahy and Abdrabou*, 2012)

Blasts and earthquakes have yielded different spectral amplitudes for the same direct wave phase at regional distances in many instances (Smith, 1989), which can be used to discriminate underground explosions from earthquakes.

In a study made by kim et al (1993) in the easter United States Pg waves from explosions have stronger high frequency content than Lg waves over the broad high frequency band 5 - 25 Hz at regional distances. It is also noted that observations in the western U.S. have been reported as having Pg/Lg higher for earthquakes than explosions(e.g., Bennett & Murphy, 1986).Therefore, Ap/As (Surface wave) amplitude ratios of waveforms are calculated in different frequency bands by removing instrument and Wood-Anderson simulated seismogram.

Spectrogram of earthquakes and quarry explosions

P and S waves from ripple-fired quarry blast shave similar frequency content and show frequency banding due to spectral modulation (Kim et,a 1993).

Spectral analysis of seismic event from earthquakes and quarry blasts

Visual inspection of the selected set of complete (body-,surface-, and coda-wave) velocigrams and of their smoothed Fourier amplitude spectra revealed frequent occurrence of surface waves with periods of about 0.2 to 0.4 sec in velocigrams of explosions from some quarries and absence of such surface waves in velocigrams of most of the micro-earthquakes, lower surface-wave amplitudes for micro-earthquakes than for quarry blasts of comparable magnitude in most cases, and systematically more high-frequency energy in the ground-velocity spectra of micro-earthquakes in comparison with those of quarry blasts of comparable magnitude (Musil & Pleginger, 1996). Delay firing in quarry sites imposes frequency cutting upon the spectra and gives spectra corner frequencies lower than those of micro-earthquakes with the same magnitude(Keith & McLaughlin, 2004).

Coda length of seismogram from earthquakes and quarry blasts

On the basis of the analysis of quarry blast and a shallow earthquake it appears that the duration as determined from the seismogram is almost two times smaller for an explosion than it is for a comparable earthquake (Dahy and Abdrabou, 2012).Seismogram of quarry sites are shorter than Earthquakes.

CHAPTER 5

DATA AND ANALYSIS

5.1 Data collected from quarry sites

The seismic activities registered around Addis Ababa are of tectonic origin earthquakes and quarry blasts around the city, and it is difficult to differentiate events from which source. One of the objectives of this research is to find a way to discriminate seismic events from the two sources. Therefore, it was necessary to collect data from quarry sites by field observation on quarry sites such as

- Location of quarry sites
- Time and date of blasts
- Amount of explosive they use for blast
- The amount of charge per hole and delay time between individual explosions is collected.

To collect such information's described above I visited the quarry sites around Addis Ababa for about 45 days from a December 10, 2016 to January 25, 2017G.C. The time it took me for field observation is longer than I planned in my proposal because of large number of quarry sites scattered in all direction around Addis Ababa city. I could not find priory information on the number and distribution and exact locations of the quarry sites. Most of the quarry sites are 10-20km far from the city and they are inaccessible for public transport, therefore I had to walk 10-20 km a day to search and access these quarry sites. I visited about 68 quarry sites around the city, out of these 48-quarry sites use explosive for excavation of rock from the ground.

5.1.1 Location of quarry sites which use explosives for mining

The location of quarries sites is determined using hand held GPS with Garmin model. The location is taken in unit of degree using the Adendan reference system.

5.1.2 Time and date of blasts by quarry sites

I tried to collect the date when they explosion took place from quarry sites. However, either most of the quarries sites do not have the data or they are not willing to provide the data. Some quarry sites have the date when the blast took place but not have the specific time of explosion. Therefore, my effort to gate the start time of quarry explosion events was a failure. Generally, what I have got from interviewing the managers of quarry sites is that they undertook their blast from 8:00 GMT to 17:00 GMT during a daytime. The blast is undergone under the supervision of security forces from government and by a specialist in mine blasting, the call him “the blaster”.

Quarry sites	**Date of explosion**	**Date of explosion**	**Date of explosion**	**Date of explosion**	**Date of explosion**
Gedeo Crasher	03/12/2016	12/12/ 2016	29/12/2016	08/01/2017	16/01/2017
Dereje crasher	07/01/2016	08/01/2016	1/01/2016	_	_
Furi -4	10/10/2014	19/09/2014	16/06/2015	17/06/2015	18/11/2016

Table 5.1 Example of data collected about date of explosions in some quarry sites

5.1.3 Amount of explosives used in a single blast

The managers in most of the quarry sites are not willing to provide me information related to explosives used in their quarry sites. They relate the inquiry with security issues. Here is in the following table what I have got from few quarry sites

Goro-2	Date of explosion	07/08/2014	12/08/2014	13/08/2014	14/08/2014	23/08/2014
	Amount of explosive	1757kg	1557kg	125kg	77kg	172kg

Table 5.2 Sample data about the amount of explosives used by quarry sites.

The amount of explosives used for a single blast varies with date in a single quarry site and it varies from quarry site to quarry site. Some active and big quarries use large amount of explosive at a time and they blast with higher frequency than small quarries.

These quarry sites use explosives sizes ranging from 50Kg to 1800kg. The method of blasting is, first they drill array of cylindrical holes with diameter of 10cm with depth that ranges from 6 to 18m. They use array of holes with 1-2m separation filled with explosives and connected by circuit igniting the blast remotely. They are set to explode remotely using the electric circuits with milliseconds of delay on each hole to control rock mass movement. It is not considered as a single explosion. Seismic sources emerge consecutively with every explosion from each hole. Thy holes are connected network of wires and the end of the wire used by the blaster to trigger the explosion.

5.2 Seismic stations used in the study and the data collected from the stations

Station	Location	Seismic sensor	Sampling frequency	Data logger	Longitude	Latitude
AAE	AAU (IGSSA)	CMG-3T (broadband)	40Hz	RT130	38^{0}45.96'E	9^{0}02.10'N
FURI	Mount Furi	STS1 (Broadband)	20Hz	Quantera 330	38^{0}40.81'E	8^{0}53.73'N
WLRA	Wolmera	Le-3d/5sec (Short period)	40Hz	RT130	38^{0}41.56'E	9^{0}05.62'N
ANKE	Ankober	Trillium compact (broad band)	40Hz	RT130	39^{0}44.51'E	9^{0}34.96'N

Table 5.3 Basic information of seismic station used for this study

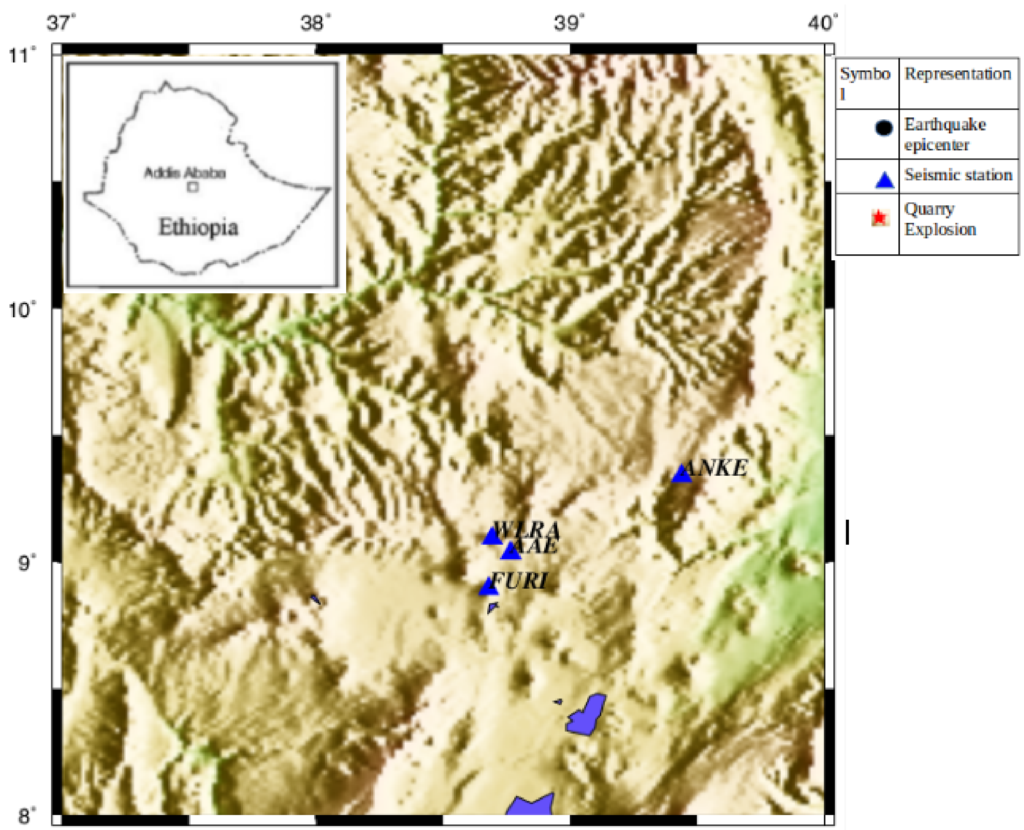

Figure 5.1 Map showing the location of seismic stations used in this study around Addis Ababa. Note that the blue triangles show the location of permanent seismic stations around the city.

WLRA seismic station

For triangulation of the location of seismic events, we need at least three seismic stations in a triangular distribution. At the beginning of this research, there were only two seismic stations in close range to Addis Ababa city. Actually, there is a third station at Ankober ANKE, which is relatively far from the Addis Ababa city to locate small quarry events near the city using this station. A third station was necessary with FURI and AAE to locate small quarry explosion events. Therefore, with my request IGGSA (Institute if geophysics space science and Astronomy) deployed a third short period permanent seismic station at Wolmera which is North West of the city center (38^{0}41.56'E, 9^{0}05.62'N) on December 05, 2016 G.C.

Figure 5.3 Photograph of the new seismic station (WLRA) at the time its deployment at Wolmera. The people seen in the picture are the researcher and staffs of the Seismology and Earthquake Engineering unit of IGSSA.

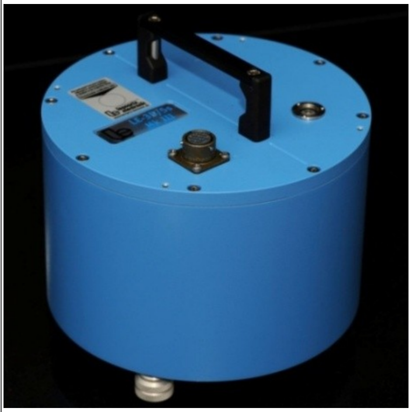	 RT130 Data Logger

Figure 5.4 the seismic sensor and data logger deployed in the new permanent seismic station at Wolmera. The sensor is short period Le-3d/5sec, with Refraction technology RT130 data logger.

The new WLRA seismic station at Wolmera is deployed on a basaltic bad rock. The short period (Le-3d/5sec seismic sensor is rested inside one meter depth excavated bedrock. This is done to decouple the seismic sensor from unwanted amplification of the incoming seismic signal due to the surrounding surface filled by soft soil. The installation of this station solves the sparse distributions of seismic stations around the city.

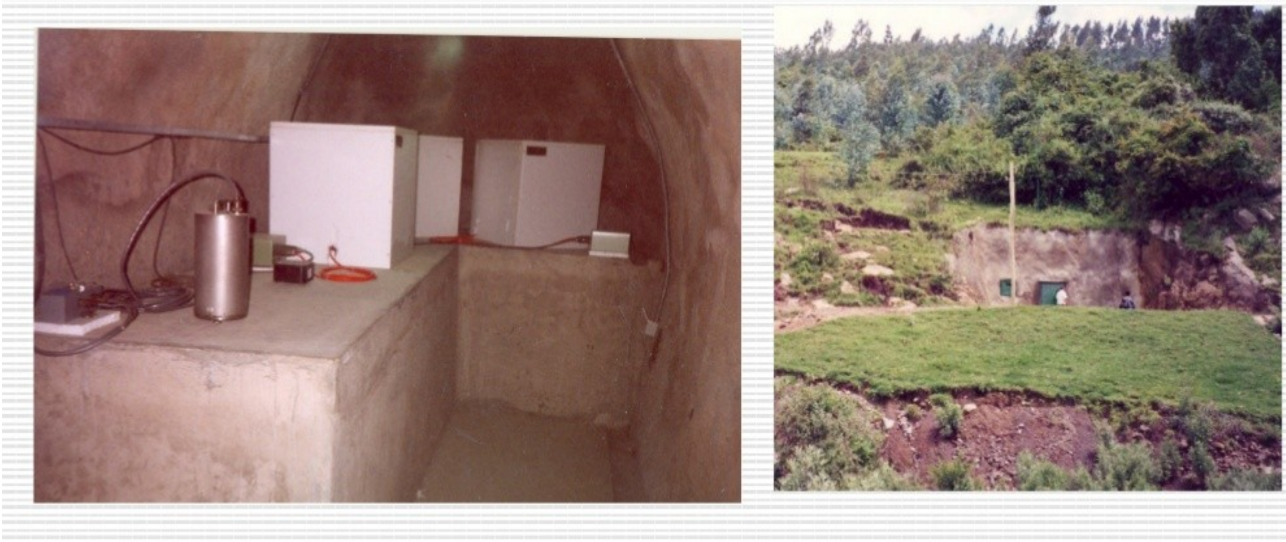

Figure 5.5 Photograph of Furi seismic stations; it is one of the three stations used in the study. It is affiliated to IRIS. It is found under an excavated cave on Mount Furi southwest of Addis Ababa city.

The second type of data collected are seismic digital data from four seismic stations around Addis Ababa city. The waveform data is collected from two three -component, broadband seismic stations located around the city with distances of 10-20km. These stations are, the AAE seismic station found in the campus of Addis Ababa university under IGSSA and the other seismic station is FURI seismic station found on Mount Furi south west of Addis Ababa. The data from these two seismic stations is collected from IGSSA seismic database.

Seismic station	**Original acquired data format by data loggers**	**Newly converted data format**
FURI	Mini-seed	SEISAN
AAE	Mini-seed	SEISAN
ANKE	Mini-seed	SEISAN
WLRA	REFTEK	SEISAN

Table 5.4 Seismic stations used in the study the type of data format they acquire data and to which data format it is converted for further analysis.

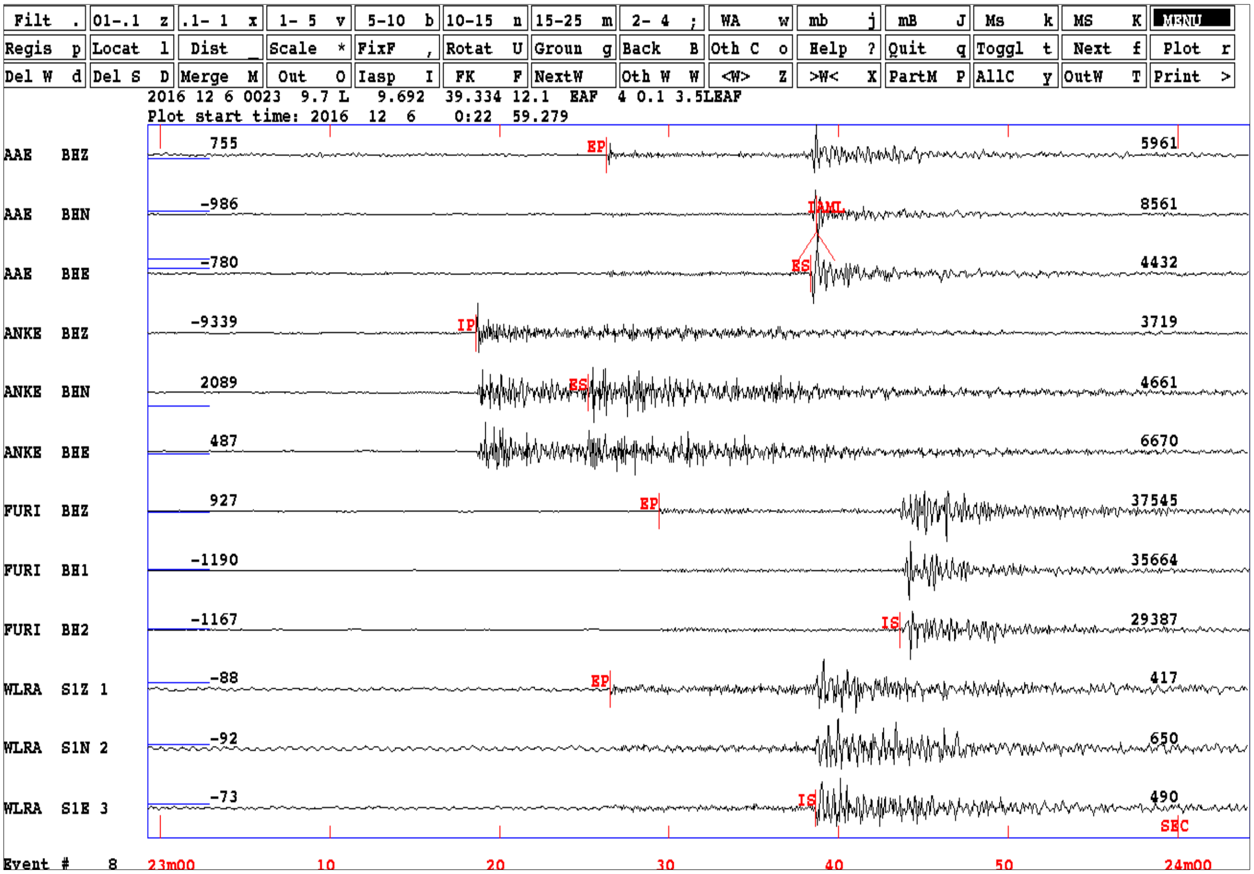

Figure 5.5 seismic signals collected and stacked from the four seismic stations using SEISAN earthquake processing software. Not that the time for arrival of P and S- phases are picked (EP in red color stand for emergent p-phase and IP means impulsive P- phase; ES means emergent S-phase and IS impulsive S-phase).

The seismic data are collected from newly deployed seismic stations (WLRA) directly from the seismic station at Wolmera. These data are converted to an appropriate data format for further processing. The amount of data collected is data

- From January 2016 to August 2017 G.C from AAE, FURI and ANKE seismic station and from December 2016 to August 2017G.C from the new WLRA station. I analyzed a period one and half year data from continuous seismic data from four seismic stations.

5.3 Seismic data analysis

5.3.1 Location of events

The following chart shows the data analysis procedure for locating seismic events followed by the this research for location of events

- Collect data from seismic stations
- Convert the data from different data format to by SEISAN data format
- Registering data to SEISAN database
- Inserting path specific travel-time corrections (crustal model), and location of the seismic stations used in the study to standard travel-time model to account of the lateral Earth structure of the locality to SATION0.DAT file of SEISAN software
- Reading the continuous data searching for seismic events
- Filtering the seismic signal using different frequency band to get clear pick for P& S arrival times
- Registering for the event with P &S pick
- Locating the registered events and saving the locations
- Plotting the epicenters of the events on GMT

5.3.2 Calculation of local magnitude (ML)

Here the procedure for calculating local magnitude used in this study

- Inserting local attenuation and other coefficient (Kier.et.al, 2006) to standard travel-time model to account of the lateral Earth structure of the locality to DAT file of SEISAN software
- Retrieving the located events from the SEISAN database
- Removing the instrument response of the signal
- Calculating local magnitude automatically (IAML) by measuring the largest amplitude from the surface wave

5.3.3 Spectrogram calculation using SAC

- Converting the selected event waveform into SAC (SEISMIC ANALYSIS CODE) format.
- Removing the instrument response of the waveform.
- Computing the FFT of the signal.
- Generating the plot for the spectrogram of the signal for the preferred frequency bands.
- Aptitude spectra of events are calculated and plotted on log-log graph.

5.3.4 Calculating Ap to ALg ratio

Procedure followed to calculate Ap/ ALg

- Removing instrument response for selected event.
- Maximum amplitudes of body wave (Ap) and surface wave (ALg) is calculated from Wood -Anderson simulated displacement seismogram.
- Amplitude ratio of body to surface (Ap/ALg) is calculated for each seismic event.
- The ratio (Ap/ALg) for events for earthquakes and quarry explosions are plotted together for comparison.

CHAPTER 6

RESULT AND DISCUSSION

6.1 Distribution of epicenters of seismic events around A/A

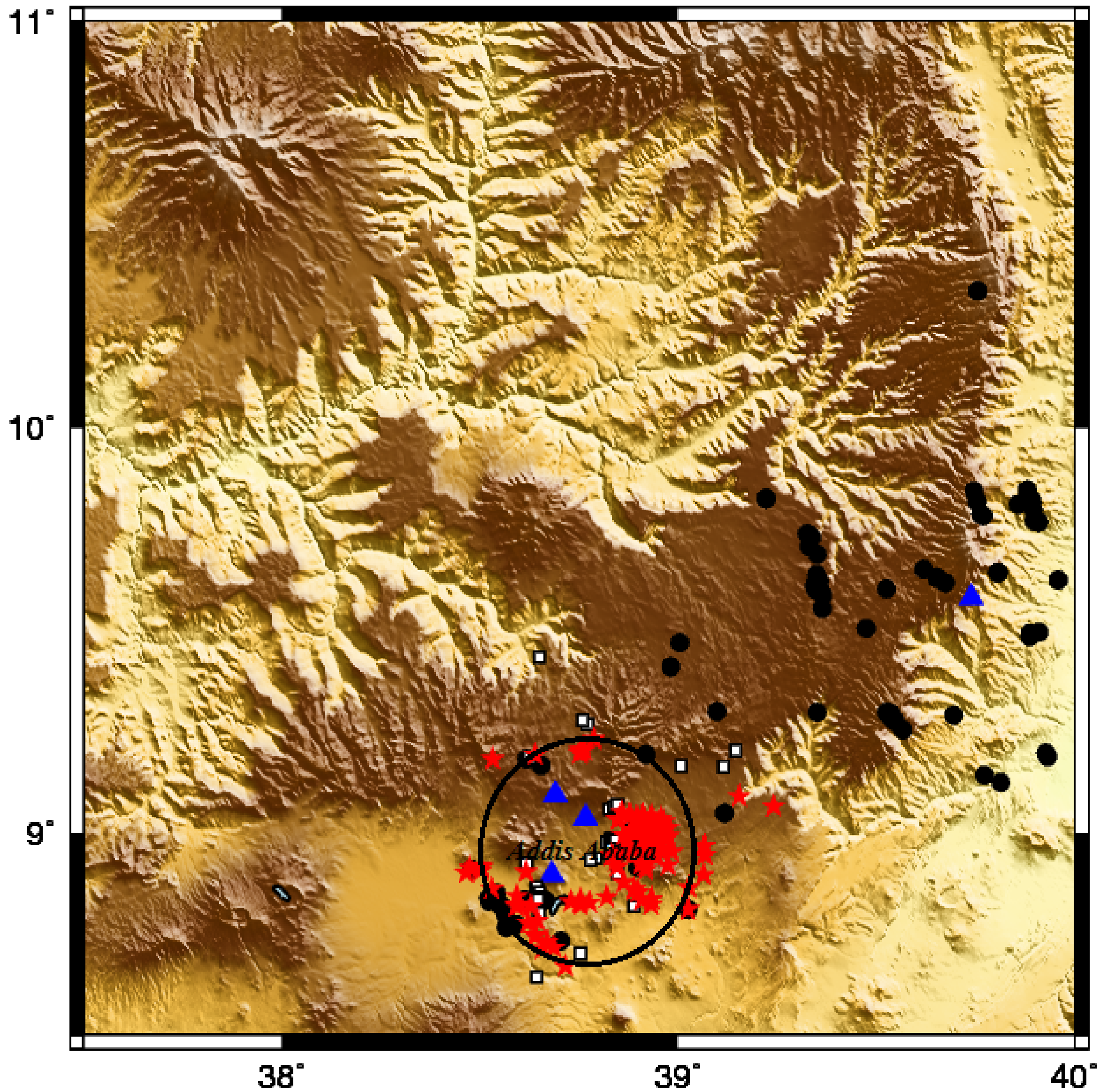

Figure 6.1 Plot of all seismic events around Addis Ababa in the study period using GMT. The white squares shows stations: blue triangles shows location of seismic stations; black circular dots shows epicenters from earthquakes and the red stars represent epicenters of quarry explosions.

The seismic activity of Addis Ababa and its surrounding is studied starting January 2016 to August 2017 using AAE, FURI and ANKE and WLRA permanent seismic stations deployed around the city. Therefore seismic activity of Addis Ababa and its surrounding is observed for the period of one and half years. During this period of the study, 204 seismic events were located in the study area with local magnitude ranging from 1.3 to 5.1 ML. The seismic events are sourced from 81 natural earthquakes and from 123 quarry blasts around the city.

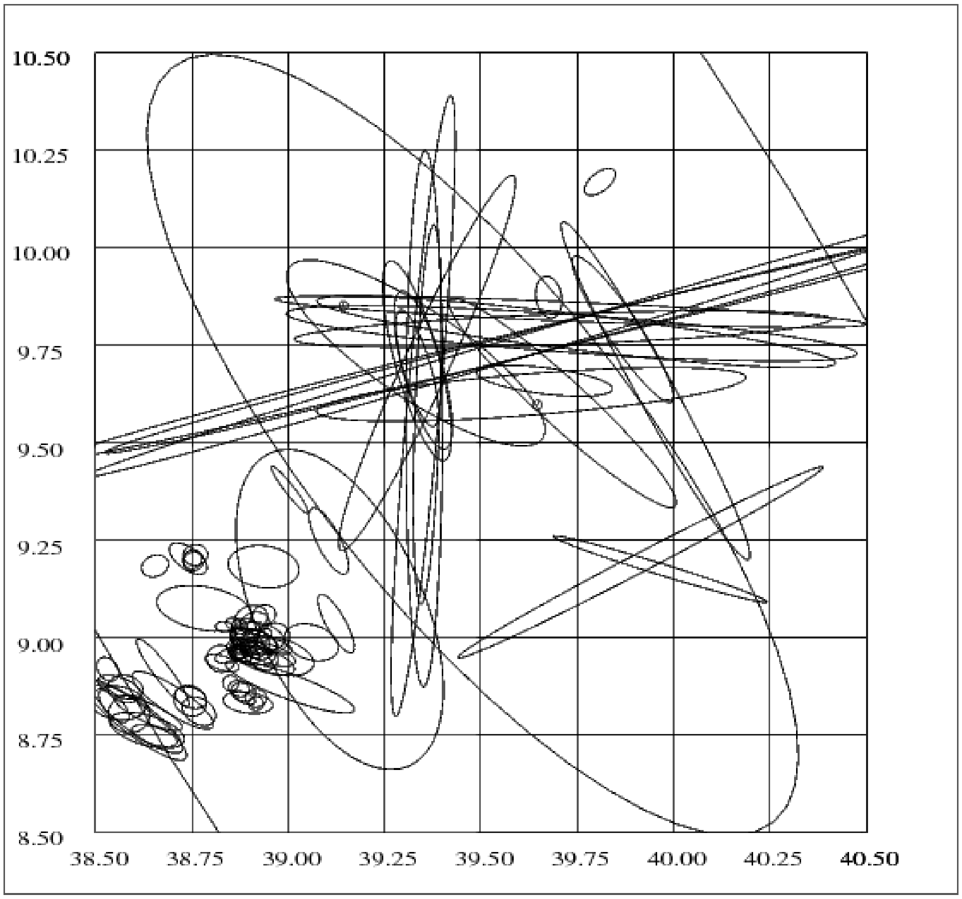

Figure 6.2. Error ellipse of some seismic events in study area.

Note that the ellipses around Addis Ababa are smaller than around Ankober area. This means the location is events is with smaller uncertainty than the Ankober area. This due to the relatively good distribution of seismic station around Addis Ababa and the events are within the network of the seismic stations.

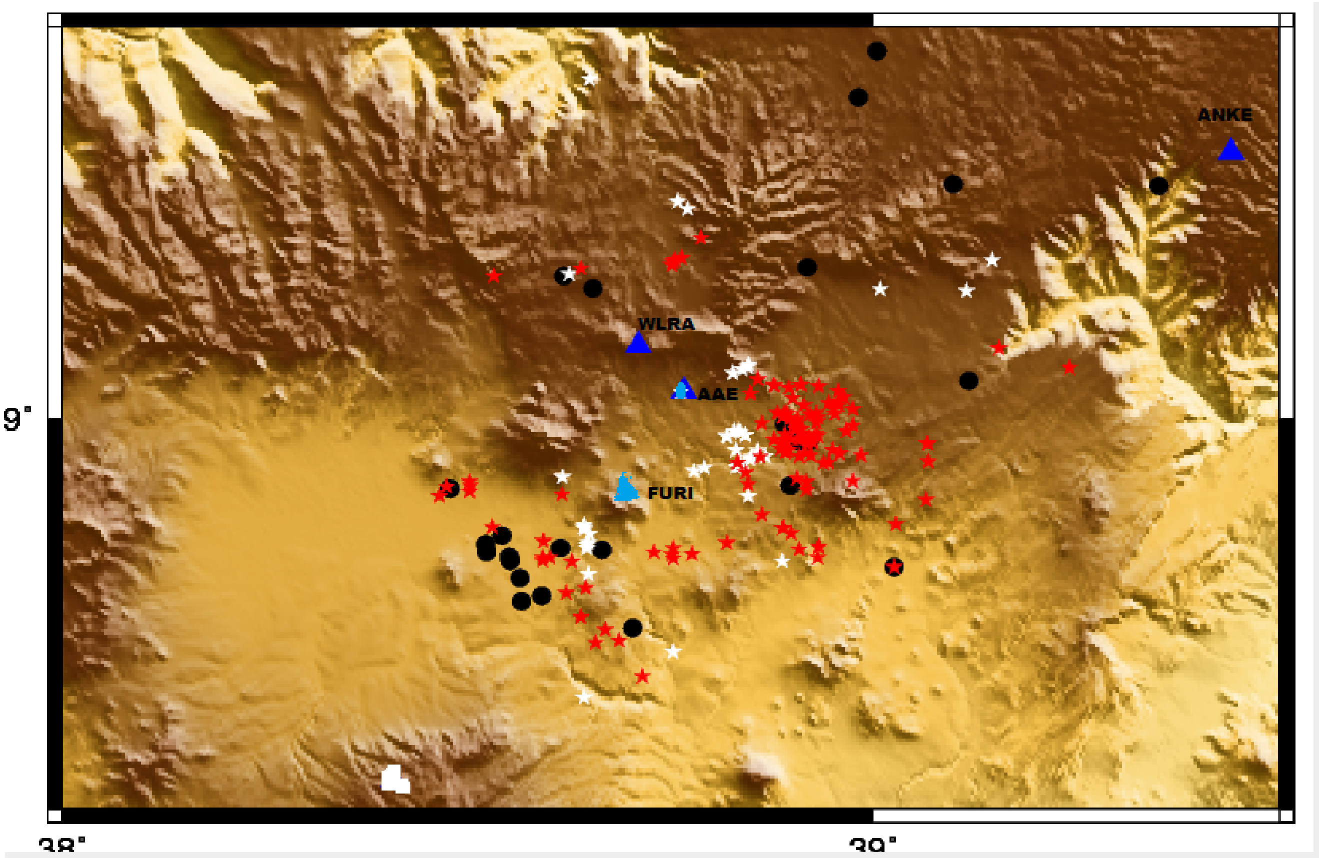

Figure 6.3 Closer look at the distribution of seismic events from quarry blasts and from earthquakes around Addis Ababa. Note that Blue triangles represent seismic stations; White stars are used for location of quarry sites and red star used to represent quarry blasts

The epicenters of the natural earthquakes as shown in the map above (Fig 6.1) are not randomly distributed. Rather their trend of distribution seems aligned with the Great rift system, which is along NE-SW direction. The earthquake events specifically near the city are preferably concentrated southwest (South of Mount Furi) and north east of the city. The events south of Mount Furi might be associated with the fault system run along Addis- Ambo-Ghedo or along with MER.

6.2 Seismic events from quarry explosions

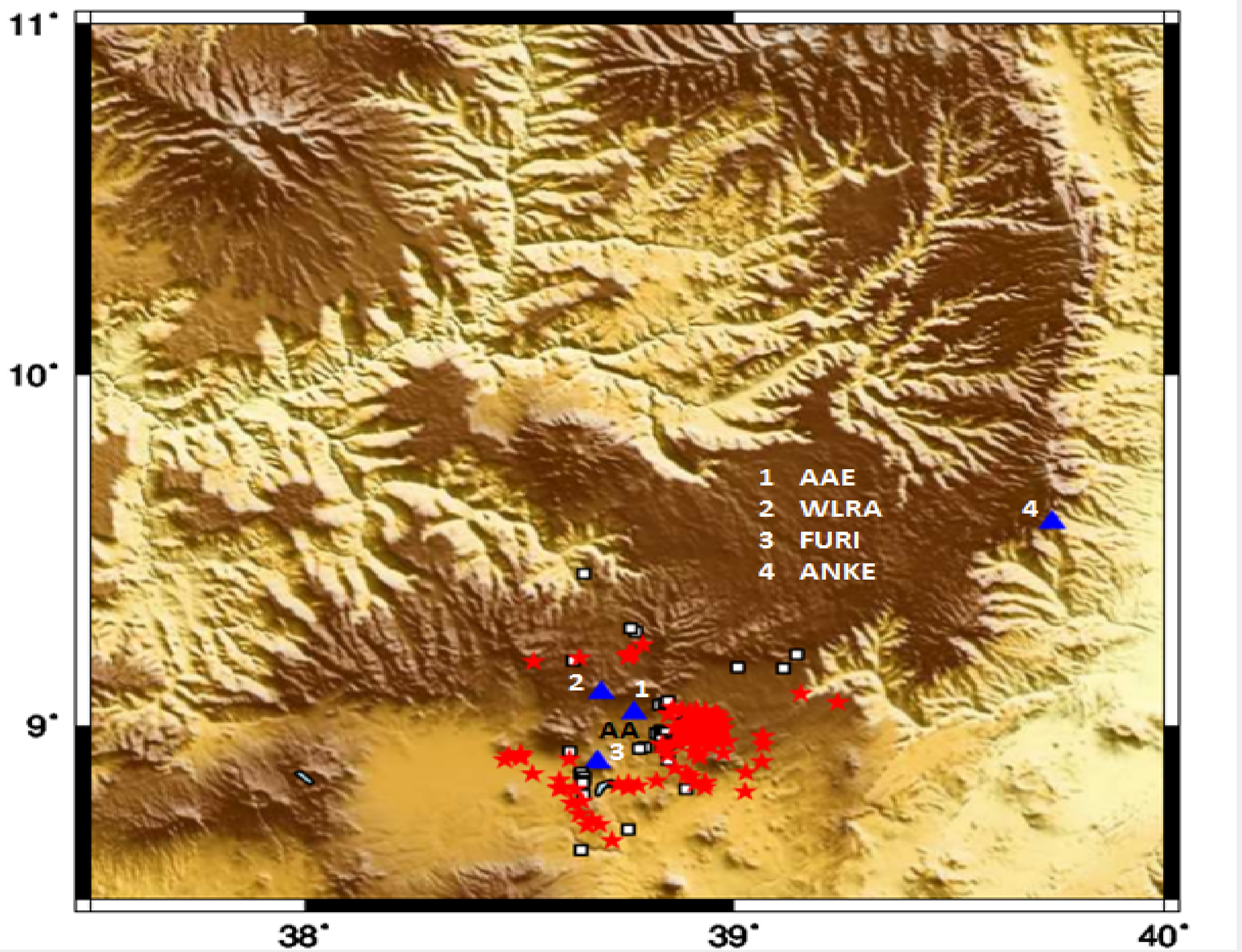

Figure 6.4 Distribution of quarry sites and explosion events for comparison. Note that Blue triangles represent seismic stations, which are designated by numbers and shown in the legend, White Square are used for location of quarry sites and red star used to represent quarry blasts.

The explosion seismic events registered are originated from 48 active quarry sites around the Addis Ababa. The events are originated from quarry blasts in quarry sites around the Addis Ababa city for mining purpose.

Our network of stations around the city does not detect most of the quarry blasts around the city. An estimated of 1000 blasts from 48 quarry sites might occurred during the study period.

However, the registered quarry explosion events from three seismic stations are 123, which is 10% of all quarry blasts. The detection capability of network of seismic station around the city is low; this might be due to the small magnitudes of explosions in the quarry sites and the relative distance of quarry sites from seismic stations. The frequency of blasts in each quarry site is from three explosions per month for some active sites to once in two months in some other quarry sites.

Some explosions may be registered in the nearby seismic station and the seismic propagation from these explosions fails to reach to all of the stations used in the study. This failure to be registered in relatively far stations is due to small amount of explosive used at a time (as small as 50kg in some quarries) and the sparse distribution of seismic stations around the quarry sites. Therefore, the quarry events located in this study should originate from such large explosions within the network seismic stations around the city. The amount of explosive used in some bigger quarry sites reach up to 1800kg explosives of different kind. The locations of the quarry sites are clustered around the city with distance of 10 to 30km from the city center. The epicenters of quarry explosions are concentrated around the city following the distribution pattern of these quarry sites.

The local magnitude of quarry explosions ranges from 1.3 to 3.0 ML. Most of the events registered from quarry explosions and natural earthquakes are classified as small seismic events.

6.3 Spectrogram of earthquakes and quarry explosions

6.3.1 Spectrogram of earthquakes

The seismogram of the signal from earthquakes contain higher amplitude first arrival with low frequency relative its surface wave. The surface waves from earthquake events have higher amplitude with higher frequency content. When we look at the seismogram of the signal from earthquakes, contain first arrival with lower frequency and higher amplitude relative to its surface wave. The surface wave from earthquakes has lower amplitude with higher frequency content relative to its body wave.

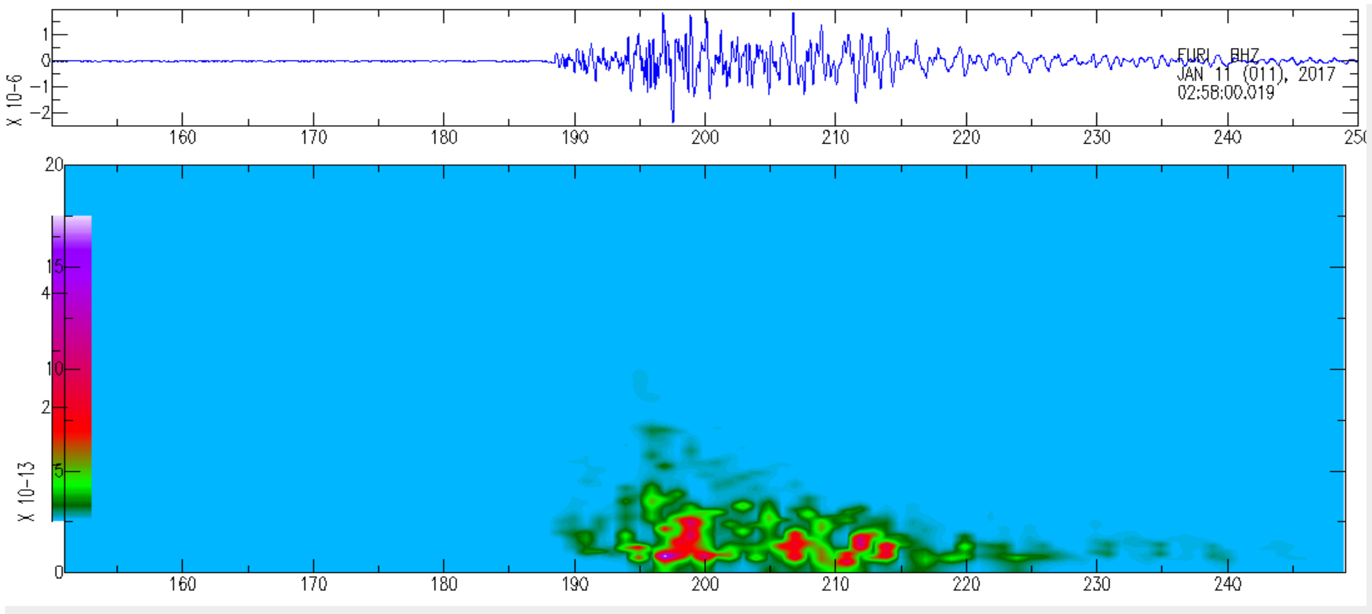

which is the color bar, shows the amplitude of the signal.

6.3.2 Spectrogram of quarry blast events

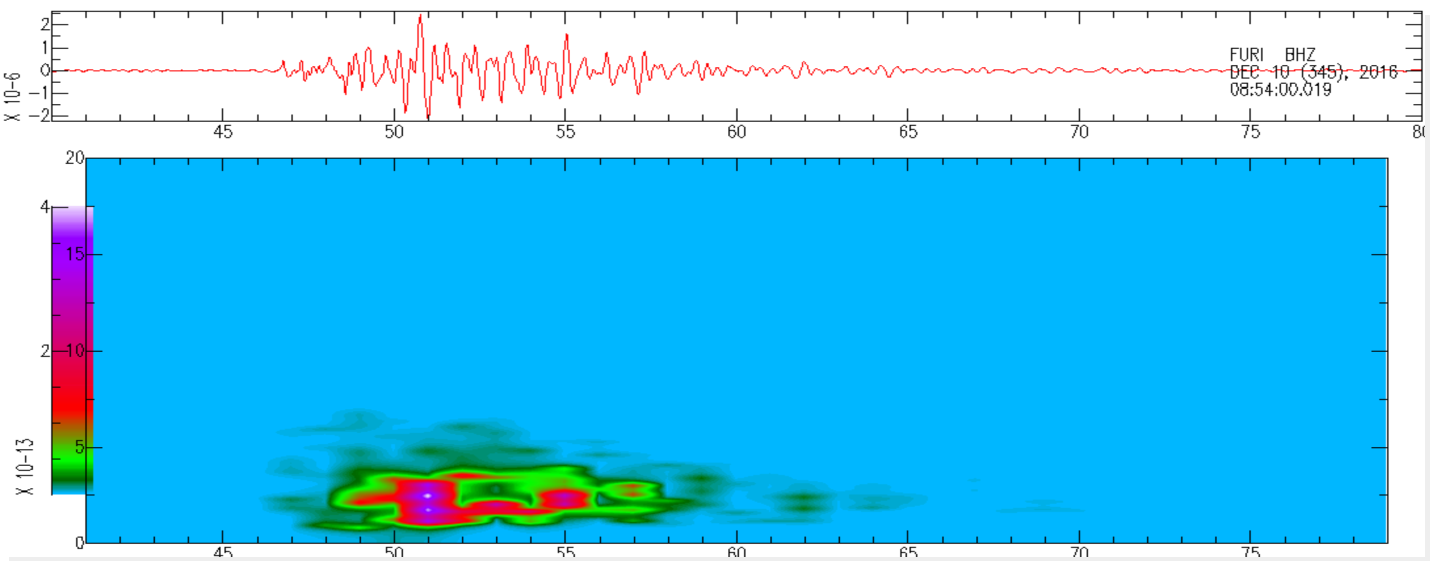

Figure 6.6. Spectrogram of quarry explosion with magnitude 2.7 ML from Z component FURI station. The map is XYZ plot of frequency range along Y-axis, time along X-axis and the Z-axis, which is the color bar, shows the amplitude of the signal.

Spectrogram from quarry blasts seem to contain weaker body wave but with higher amplitudes surface waves relative to earthquakes. The spectrogram from quarry blasts contain body waves with higher frequency content but with weak first arrival and surface waves with higher amplitudes relative to earthquakes. This weak first arrival on quarry blasts unlike single explosion may be due multiple source explosions with milliseconds of delay between subsequent explosions.

6.4 Amplitude of body wave (Ap) to surface waves (Alg) ratio

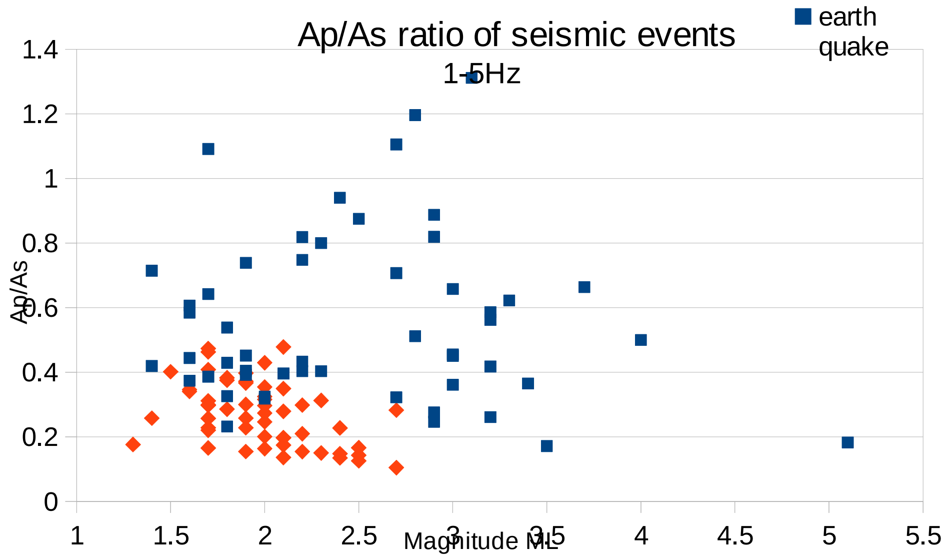

(a)

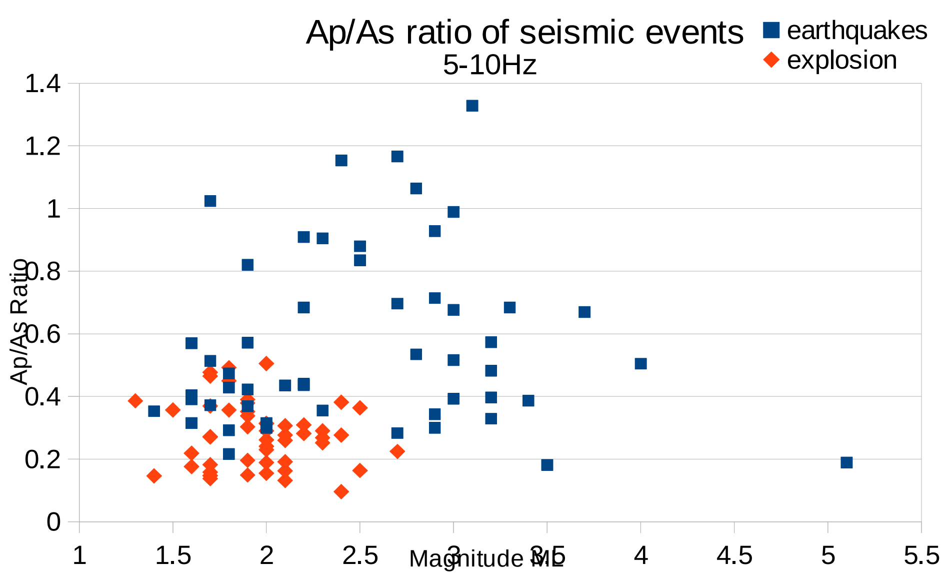

(b)

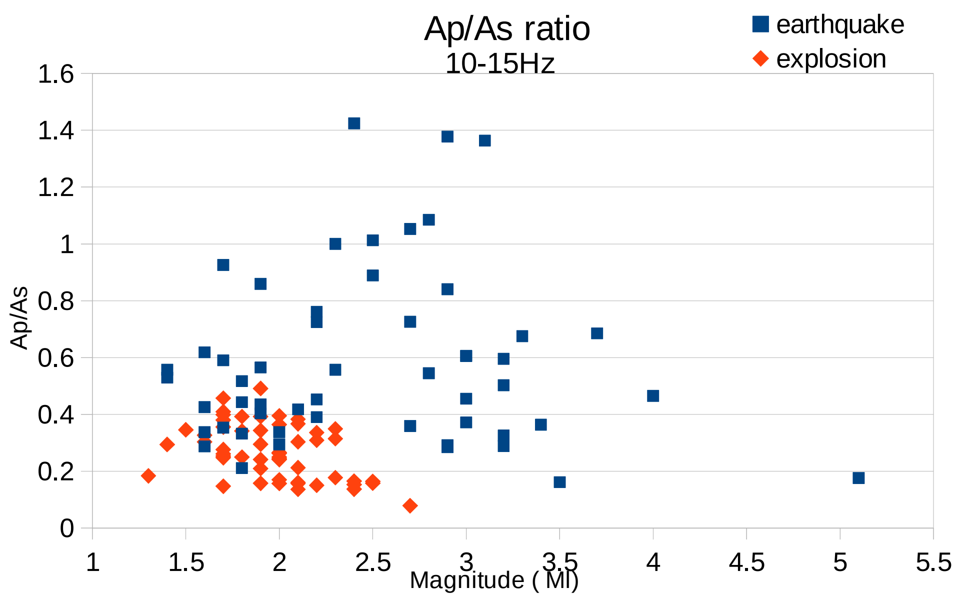

(c)

Figure6.7 Chart showing amplitude ratio (Ap/As of body wave to surface wave for 50 quarry explosion and 50 earthquake events for different frequency bands (a),(b) and (c).

Ap/As ratio for earthquakes look higher than those quarry explosions whereas the Ap/As ratio for quarry explosions are smaller than earthquakes. This may be due to the weak first arrival in quarry explosions relative to its surface wave. The calculated Ap/ALg ratio from earthquakes and quarry blasts shows that natural earthquakes seem to have higher ratio than explosions, with no variation in frequency.

The distinction between the two events seems do not affected by frequency. We noticed that the detonation of the TNTs at the quarry sites is done with a ripple trigger approach, which does not give strong P arrival at the recording stations, and it is found to be weak. The Ap/ As ratio has no 100% efficiency to discriminate between the two groups of events.

6.5 Spectral analysis of seismic event from earthquakes and quarry blasts

(a) spectra of an earthquakes

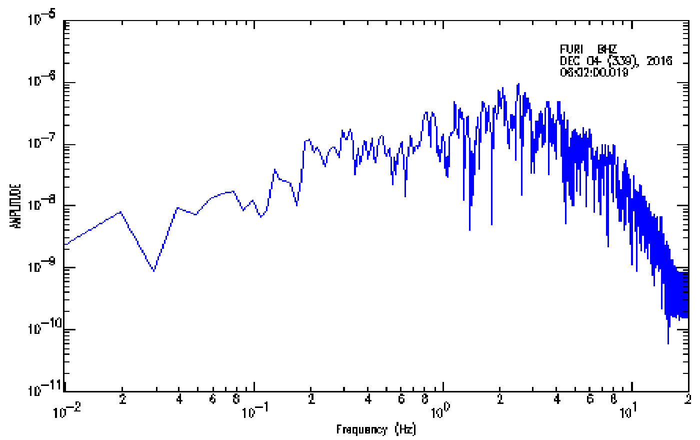

(b) Spectra of an explosion

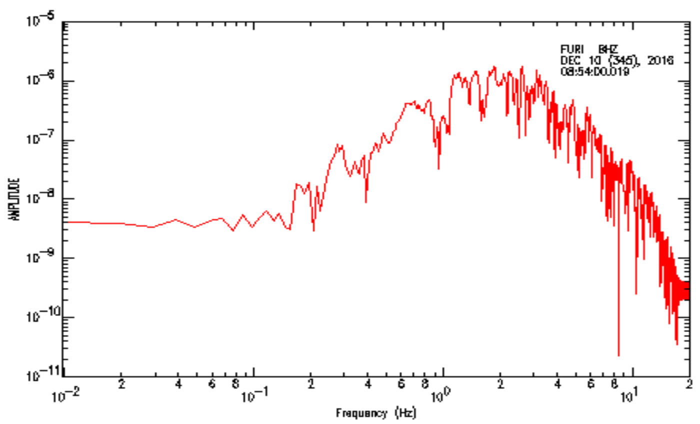

Figure 6.8 spectra of an earthquake and a quarry blast (b) with comparable magnitude

Seismogram of the signals calculated by filtering the signal in the frequency range of 1-10Hz (Nyquist frequency for FURI) using SAC. A significant difference was found by comparing the spectra between earthquakes and quarry blasts. The curves of power spectra verses frequency for blasts decrease more sharply than earthquakes at high frequencies.

6.6 Coda length of seismograms from quarry blasts and earthquakes

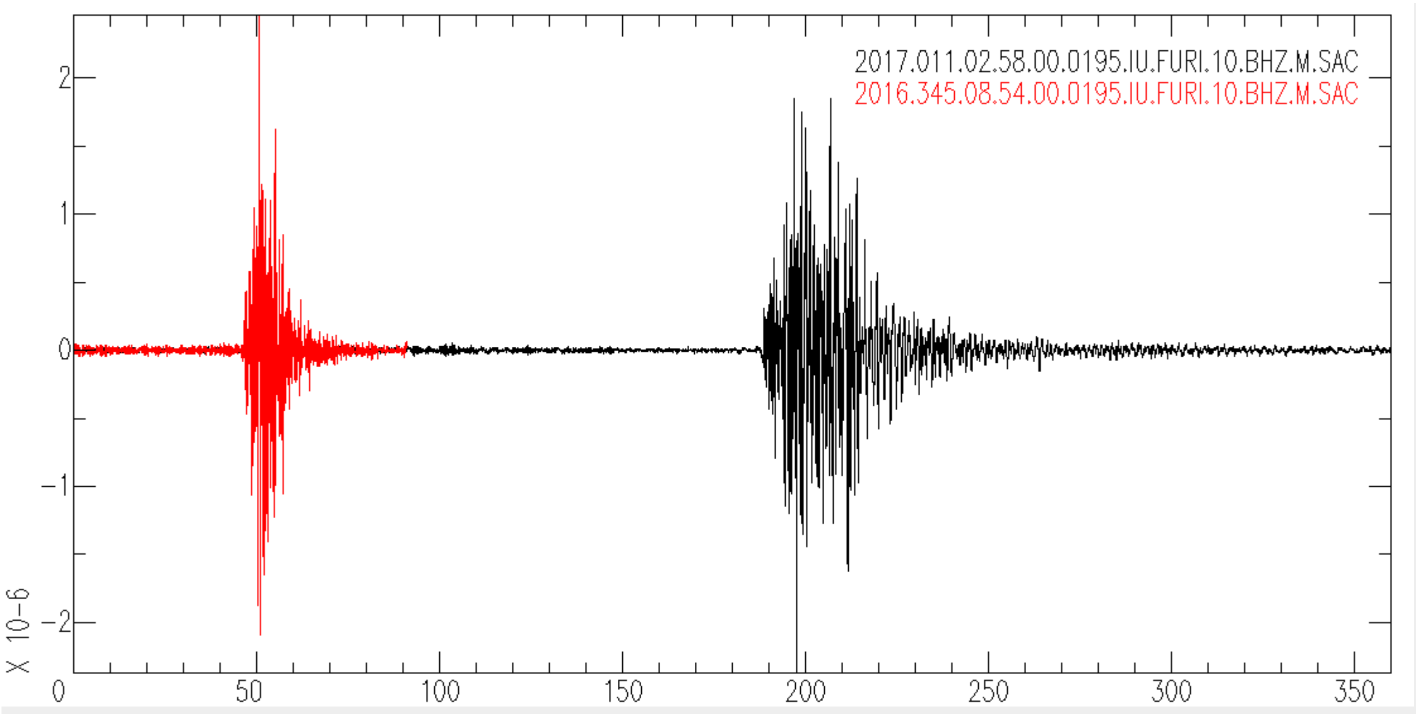

Figure6.9 Seismogram from an earthquake (Black) and a quarry blast (red) with ML 2.8 and 2.7 respectively from approximately the same distance from FURI station

The coda lengths of quarry explosion seismograms are shorter than earthquakes with comparable magnitude and travel path.

CHAPTER 7

CONCLUSION

This study shows that, there is significant number of seismic activities due to tectonic origin and quarry blasts around Addis Ababa with magnitudes ranging from 1.3 to 5.1ML.

The seismic events both the natural and those from quarry explosions are clustered around the city of Addis Ababa. During this period of study most of the events from natural earthquakes around the city are concentrated following the trend of the MER which is trending NE -SW. Few events are seen on north of the city and around its eastern part. Events are not located within and on the western side of the city within the period of the study.

The epicenters of events from quarry explosions are scattered in close proximity to the city trending with location of quarry sites. Except the western part of the city, quarry sites are clustered within a radius of 10-30 Km from the city center. Locations of epicenter from quarry blasts correlated with the location of quarry sites. Most of the epicenters from explosions concentrated east of the city due to location of most active quarry sites in this part of the city.
Most of the quarry explosions around city are not detected with the exception of larger explosions. This might be related to small explosion sources or due to sparse distribution of seismic stations.

Most of the origin time of events from quarry explosions occurring around the city is in day time between 8:00 AM to 5:00PM. Unlike explosions, the earthquake origin time is not limited to certain range of time.

The curves of power spectra verses frequency for blasts decrease more sharply than earthquakes at high frequencies.

The calculated Ap/ALg ratio from earthquakes and quarry blasts shows that natural earthquakes seem to have higher ratio than explosions, with no variation in frequency.

The coda lengths of quarry explosion seismograms are shorter than earthquakes with comparable magnitude and travel path.

CHAPTER 8

RECOMMENDATION

The sites of quarry explosions are in some places very near to residential areas, buildings and public areas. This may cause damage to the nearby residential buildings and other infrastructures.

Therefore, the location of the quarry sites and their effect on the built structures should be investigated relation to amount of explosive and relative distance.

More seismic stations should be deployed for detail investigation of the quarry blast effects and seismicity around Addis Ababa city as Addis is the seat of the African Union and is one of the fastest growing cities in Sub-Saharan Africa.

References

Abebe, M. (2010). Disaster management in Ethiopia: A review of its checkered history, its transformation and some implications for a vibrant disaster management system, 1975–2008. Journal of Sustainable Development in Africa. 12(4), 237-254.

Assegid Getahun, 2007. The geology of Addis Ababa City. Ministry of mine and energy, Geological Survey of Ethiopia. Addis Ababa. pp. 12-25

Atalay Ayele, 2010. The September 19, 2009 M_l 5.0 earthquake in the Ankober area: lessons for seismic hazard mitigation around Addis Ababa. Africa Array Workshop 2010 – Abstracts

Atalay Ayele, 2017.Probabilistic seismic hazard analysis (PSHA) for Ethiopia and them neighboring region. Journal of African Earth Sciences pp. 257-264

Bennett, T. J. and J. R. Murphy, Analysis of seismic discrimination capabilities using regional data from western United States events, Bull. Seism. Soc. Am.,76, 1069-1086, 1986

Bowers, D., and Walter, W. R., 2002. Discriminating between large mine collapses and explosions using teleseismic P Waves. Pure and Applied Geophysics, 159, 803–830.

Bowers, D., and Selby, N. D., 2009. Forensic Seismology and the Comprehensive Nuclear-Test-Ban Treaty. Annual Reviews of Earth and Planetary Sciences, 37, 209–236.

Dahlman, O., Mykkeltveit, S., and Haak, H., 2009. Nuclear Test Ban: Converting Political Visions to Reality. Berlin: Springer.

Dahy, S.A. and G.H. Hassib, 2010. Spectraldiscrimination between blasts and microearthquakes in southern Egypt. Res. J. Earth Sci., 2(1): 01-07.

Fekadu Kebede, 1996. "Seismic Hazard Assessment for the Horn of Africa", Proceedings of the Ethiopian Association of Seismology and Earthquake Engineering (EASEE) on Seismic Hazard Assessment and Design of Structures for Earthquake Resistance, Addis Ababa, Ethiopia, pp 25-38, Addis Ababa, Ethiopia.

Geiger, L. (1912). Probability method for determination of earthquake epicenters from the arrival times only. Bull. St. Louis Univ. 8,60-71.

Gitterman, Y., V. Pinsky, and A. Shapira (1998). Spectral classification methods in monitoring small local events by the Israel seismic network, J. Seismol. 2, no. 2, 237–256.

Gouin, P.(1979). Earthquake history of Ethiopia and the Horn of Africa. International Development Research Centre (IDRC), Ottawa, Ontario, pp.258.

Gutenberg, B. and C.F. Richter, 1956. Magnitude and energy of earthquakes, Ann. Geofis., 9: 115.

Hartse, H. E., W. S. Phillips, M. C. Fehler, and L. S. House (1995). Single-station spectral discrimination using coda waves, Bull. Seismol. Soc.Am. 85, no. 5, 1464–1474.

Hussein, A.I., 1994. Comparison of body- wave spectra of artificial and natural earthquakes in proceeding of 3 rd Scientific General Meeting B, NRIAG, Egypt, pp: 1730.

IDNDR RADIUS Project, September 1999 .Addis Ababa Case Study, Final Report. Prepared by Addis Ababa RADIUS Group.

Jens Havskov. P. Bormann, J. Schweitzer, 2011.Seismic source location. Information Sheet DOI: 10.2312/GFZ. NMSOP-2_IS_11.1

Klein, F. (2002). User's Guide to HYPOINVERSE-2000, a Fortran program to solve for earthquake locations and magnitudes, USGS, Open File Report 02-171,123pp.

Kulhanek, Ota, 1990, Anatomy of Seismograms: Amsterdam, The Netherlands, Elsevier Science Publishers B. V., 178 p.

Keir, D., Stuart, G. W., Jackson, A. & Ayele, A. 2006.Local earthquake magnitude scale and seismicity rate for the Ethiopian rift. Bulletin of the Seismological Society of America, 96, 2221–2230.

Kim, W. Y., D. W. Simpson and P. G. Richards, High-frequency spectra of regional phases from earthquakes and chemical explosions, 96pp., PL-TR-91-2285, 1991.

Kim, W. Y., D. W. Simpson and P. G. Richards,1993. Discrimination of earthquakes and explosions in the eastern united states using regional high-frequency data.geophysical research letters, vol. 20, no. 14, pages 1507-1510,

Keranen K., Klemperer S.L, Gloaguen R. and EAGLE Working group(2004). Three- dimensional seismic imaging of a protoridge axis in the Main Ethiopian rift. Geological society of America, Geology 2004;32;949-952

Khalturin, V. I., Rautian, T. G., and Richards, P. G., 1998. The seismic signal strength of chemical

Laike Mariam Asfaw, 1992, “Seismic Risk at a Site in the East African Rift System”, Tectonophysics, 209, pp 301-309.

Laike Mariam Asfaw,1985. “Seismicity and Seismic risk in Addis Ababa region” Bull, Geophysical Observatory, Addis Ababa,

Lay, T. and T. C. Wallace (1995). Modern global seismology, 521 pp., Academic Press.

Lienert, B. R. and J. Havskov (1995). A computer program for locating earthquakes both locally and globally. Seismological Research letters, 66, 26-36.explosions. Bulletin of the Seismological Society of America, 88, 1511–1524.

Miloslav Musil and A.,Pleginger August 1996. Discrimination between Local Micro earthquakes and Quarry Blasts by Multi-Layer Perceptrons and Kohonen Maps , Bulletin of the Seismological Society of America, Vol. 86, No. 4, pp. 1077-1090,

OTA, 1988. Office of Technology Assessment, Congress of the United States, Seismic Verification of Nuclear Testing Treaties, OTA-ISC-361. Washington: U.S. Government Printing Office.

Paul G. Richards, Zhongliang Wu, 2011. Encyclopedia of solid earth geophysics, National Geophysical Research Institute Council of Scientific and Industrial Research ,Hyderabad India pp. 1144-1156

Prieto, G., P. M. Shearer, F. L. Vernon, and D. Kilb (2004). Earthquake source scaling and self-similarity estimation from stacking P and S spectra, J. Geophys. Res. 109, B08310, 10.1029/2004JB003084.

Samuel Kinde, 2002. Earthquake Risks in Addis Ababa and other Major Ethiopian Cities - Will the Country be Caught Off-guarded? Addis Ababa, Ethiopia pp. 1-2

Sayed A. Dahy and Gad E. Abdrabou, 2012.Spectral Studies of Quarry Blasts and Earthquakes in Eastern Cairo, Egypt, Research Journal of Earth Sciences 4 (2): 56-62, 2012

Stain S., and M., Wysession(2003). An Introduction Seismology, Earthquakes, and Earthquake structure Blackwell Publishing Ltd. 29 pp.

Smith, A.T., 1989. High- Frequency seismic observations and models of chemical explosions; implication for discrimination of ripple- fired mining blasts, Bull. Seism. Soc. Am., 79: 1089-1110.

Smith, A. T. (1993). Discrimination of explosions from simultaneous mining blasts, Bull. Seismol. Soc. Am. 83, no. 1, 160–179.

Shearer, P., G. Prieto, and E. Hauksson (2006). Comprehensive analysis of earthquake source spectra in southern California, J. Geophys. Res. 111, B06303, doi 10.1029/2005JB003979.

Stefanie J. Baxter, 2000. Earthquake basics,Special publication no. 23, Delaware geological survey, state of Delaware , pp1-3

Su, F., K. Aki, and N. N. Biswas (1991). Discriminating quarry blasts from earthquakes using coda waves, Bull. Seismol. Soc. Am. 81, no. 1,162–178.

Richards, P. G., 1988. Seismic methods for verifying test ban treaties. In Schroeer, D., and Hafemeister, D. (eds.) Chapter 4 of Nuclear Arms Technologies in the 1990's. AIP Conference Proceedings. New York: American Institute of Physics, Vol. 178, pp. 54–108.

Taylor, S. R., N. W. Sherman, and M. D. Denny (1988). Spectral discrimination between NTS explosions and western United States earthquakes at regional distances, Bull. Seismol. Soc. Am. 78, no. 4, 1563–1579.

Tilahun Mammo, 2005. Site-specific ground motion simulation and seismic response analysis at the proposed bridge sites within the city of Addis Ababa, Ethiopia. Engineering Geology 79(2005) 127-150

Vitaly I. Khalturin, Tatyana G. Rautian, and Paul G. Richards, December 1998.The Seismic Signal Strength of Chemical Explosions, Bulletin of the Seismological Society of America, Vol. 88, No. 6, pp. 1511-1524,

Waldhauser,G. , F., Schaff, D., and Kim, W.-Y., 2006. The applicability of modern methods of earthquake location. Pure and Applied Geophysics, 163, 351–372.

Walter, W.R., K.M. Mayeda and H.J. Patton, 1995. Phase and spectral ratio discrimination between NTS earthquakes and explosions. Bull. Seism. Soc. Am., 85: 1050-1067.

Appendix I

Location of quarry sites which use explosives for quarrying around Addis Ababa.

No	Quarry name	Latitude(^{0})	Longitude(^{0})
1	Akaki1	8.9369^{0}N	38.7912^{0}E
2	Akaki2	8.9328^{0}N	38.7783^{0}E
3	Alleltu 1	9.2022^{0}N	39.1457^{0}E
4	Alleltu 2	9.1629^{0}N	39.1141^{0}E
5	Alemgena	8.9250^{0}N	38.6166^{0}E
6	Awash	8.7015^{0}N	38.7527^{0}E
7	Casma	9.1846^{0}N	38.6249^{0}E
8	Chancho 1	9.2773^{0}N	38.7585^{0}E
9	Chancho 2	9.2678^{0}N	38.7706^{0}E
10	Derba	9.4333^{0}N	38.6499^{0}E
11	Entoto	9.0579^{0}N	38.8261^{0}E
12	Entoto 1	9.0629^{0}N	38.8380^{0}E
13	Entoto 2	9.0654^{0}N	38.8448^{0}E
14	Entoto 3	9.0689^{0}N	38.8457^{0}E
15	Furi 1	8.8591^{0}N	38.6440^{0}E
16	Furi 2	8.8608^{0}N	38.6425^{0}E
17	Furi 3	8.6429^{0}N	38.6429^{0}E
18	Furi 4	8.8638^{0}N	38.6430^{0}E
19	Furi 5	8.8521^{0}N	38.6496^{0}E

20	Furi 6	8.8410^0N	38.6483^0E
21	Furi 7	8.8383^0N	38.6465^0E
22	Furi 8	8.8011^0N	38.6484^0E
23	Gelan 1	8.8174^0N	38.8874^0E
24	Gelan 2	8.8538^0N	38.8164^0E
25	Gelan 3	8.8608^0N	38.8249^0E
27	Gelan 4	8.8583^0N	38.8649^0E
28	Gelan 5	8.8597^0N	38.8306^0E
29	Goro 1	8.9776^0N	38.8186^0E
30	Goro 2	8.9765^0N	38.8193^0E
31	Goro 3	8.9842^0N	38.8279^0E
32	Goro 4	8.9838^0N	38.8332^0E
33	Goro 5	8.9822^0N	38.8355^0E
34	Goro 6	8.9790^0N	38.8415^0E
35	Goro 7	8.9790^0N	38.8415^0E
36	Goro 8	8.9592^0N	38.8301^0E
37	Goro 9	8.9516^0N	38.8663^0E
38	Moriam	9.1655^0N	39.0078^0E
39	Yerer 1	8.9583^0N	38.8566^0E
40	Yerer 2	8.9504^0N	38.8499^0E
41	Yerer 3	8.9483^0N	38.8471^0E

42	Yerer 4	8.9006^0N	38.8452^0E
43	Yerer 5	8.9420^0N	38.8398^0E
44	Yerer 6	8.9396^0N	38.8357^0E
45	Yerer 7	8.9393^0N	38.8339^0E
46	Yerer 8	8.938^0N	38.8302^0E
47	Yerer 9	9.0341^0N	38.762^0E
48	Zelalem	8.8342^0N	38.6466^0E

Appendix II

Catalog of seismic events between January 2016 to August 2017 around Addis Ababa

Year	Date	HRMM	Sec	Lat	Long	NST	rms	M_L
2016	1 5	0948	35.1	9.651	39.619	3	0.1	2.4
2016	224	0256	16.5	9.617	39.674	3	0.3	2.5
2016	3 8	1102	26.5	9.469	39.004	3	0.8	2.3
2016	410	0627	51.8	9.624	39.959	3	0.3	3.2
2016	410	1552	47.1	9.787	39.763	3	0.2	4.0
2016	410	1729	48.1	9.783	39.770	3	0.2	3.2
2016	412	0047	1.4	9.818	39.754	3	0.2	2.9
2016	423	0752	4.9	11.043	40.010	3	0.7	3.7
2016	511	0855	5.9	9.166	38.654	3	0.2	2.2
2016	530	0847	32.0	8.850	38.542	3	0.2	1.7
2016	6 4	1153	31.7	9.410	38.981	3	0.1	2.2
2016	610	0806	21.2	8.796	38.564	3	0.2	2.0
2016	617	0656	27.9	9.182	38.618	3	0.5	1.9
2016	7 9	0946	48.2	8.839	38.522	3	0.2	1.8
2016	724	2033	58.8	9.196	39.928	3	0.3	2.8
2016	731	0336	24.8	9.188	39.932	3	0.2	3.1
2016	812	0844	55.7	9.335	40.030	3	0.2	2.8
2016	820	1247	36.6	9.493	39.888	3	0.4	2.7
2016	820	1430	5.0	9.495	39.911	3	0.5	3.0
2016	9 3	1620	10.4	9.484	39.887	3	0.4	3.2
2016	910	1014	29.3	8.829	38.523	3	0.1	2.0
2016	1025	0712	50.3	8.910	38.478	3	0.3	1.6

2016 1118 0036 44.6 9.374 40.342 3 0.6 2.9

2016 12 1 0728 27.7 9.048 39.117 3 0.3 2.2

2016 12 1 1344 16.7 9.600 40.011 3 0.2 3.0

2016 12 1 1344 16.6 9.548 40.014 3 0.4 2.8

2016 12 4 0156 12.1 9.593 39.360 3 0.3 5.1

2016 12 4 0200 46.4 9.625 39.350 3 0.3 3.8

2016 12 4 0208 54.8 9.554 39.363 3 0.6 3.9

2016 12 4 0232 7.1 9.617 39.347 3 0.2 3.5

2016 12 4 0242 9.7 9.282 39.537 3 0.3 3.0

2016 12 4 0307 47.2 9.628 39.350 3 0.2 2.6

2016 12 4 0333 52.3 9.253 39.566 3 0.3 2.5

2016 12 4 0342 44.9 9.636 39.349 3 0.2 2.2

2016 12 4 0401 56.8 9.275 39.547 3 0.5 2.4

2016 12 4 0416 10.5 9.587 39.364 3 0.2 2.7

2016 12 4 0443 39.0 9.295 39.528 3 0.5 2.8

2016 12 4 0506 27.7 9.605 39.355 3 0.2 2.7

2016 12 4 0601 51.4 9.284 39.542 3 0.4 3.0

2016 12 4 0624 39.6 9.610 39.344 3 0.1 3.3

2016 12 4 0631 28.4 9.602 39.351 3 0.2 3.2

2016 12 4 0722 3.4 9.297 39.525 3 0.5 2.6

2016 12 4 1017 24.7 9.295 39.535 3 0.5 3.2

2016 12 4 2118 5.9 9.601 39.346 3 0.2 3.4

2016 12 5 1610 9.7 9.621 39.356 3 0.3 2.7

2016 12 6 0023 9.5 9.707 39.330 4 0.1 2.7

2016 12 6 0152 35.1 9.729 39.337 4 0.2 2.4

2016 12 6 0826 22.6 8.960 38.949 3 0.1 1.9

2016 12 6 0833 7.2 8.956 38.916 3 0.3 1.6

2016 12 6 1547 33.7 9.738 39.325 4 0.2 2.2

2016 12 7 0632 38.2 8.991 38.974 3 0.2 2.1

2016 12 7 1339 32.4 8.822 38.931 3 0.1 1.9

2016 12 8 0724 1.8 9.032 38.883 3 0.4 1.8

2016 12 9 0812 33.1 8.944 38.944 3 0.2 2.0

2016 12 9 1832 31.0 10.336 39.756 4 0.4 3.1

2016 1210 0854 42.4 8.746 38.639 3 0.2 1.8

2016 1210 1007 34.7 8.967 38.887 3 0.0 1.3

2016 1211 0343 48.1 9.642 39.807 4 0.1 2.4

2016 1212 0848 37.9 8.810 39.025 3 0.2 2.0

2016 1212 1844 50.6 9.767 39.909 4 0.2 2.3

2016 1213 0705 29.4 8.987 38.904 3 0.1 1.9

2016 1213 1033 7.3 8.860 38.888 3 0.1 1.4

2016 1213 1157 26.5 9.043 38.910 3 0.1 1.7

2016 1214 0854 50.9 8.968 39.066 3 0.3 2.7

2016 1215 1022 46.5 8.836 38.932 3 0.1 1.7

2016 1215 1918 40.4 9.825 39.222 3 0.2 2.6

2016 1216 0730 23.9 9.042 38.877 3 0.1 1.6

2016 1217 0838 31.0 9.032 38.848 3 0.1 1.6

2016 1219 1126 24.5 8.957 38.891 3 0.1 1.6

2016 1219 1248 54.8 8.984 38.966 3 0.3 2.0

2016 1220 0838 31.3 8.944 38.832 3 0.2 1.5

2016 1220 0859 27.7 8.980 38.890 3 0.1 1.5

2016 1221 0402 11.7 9.621 39.362 4 0.3 2.9

2016 1221 0759 37.3 9.630 39.652 4 0.2 2.5

2016 1221 1333 26.4 8.973 38.877 3 0.3 2.5

2016 1222 1516 23.6 9.669 39.698 4 0.2 2.3

2016 1223 0738 46.3 9.017 38.957 3 0.1 2.0

2016 1224 1125 6.8 8.943 38.938 3 0.2 2.5

2016 1226 0810 57.5 8.989 38.905 3 0.2 2.1

2016 1227 0742 16.5 9.007 38.883 3 0.1 1.6

2016 1227 0932 28.1 8.853 38.898 3 0.1 2.0

2016 1227 1038 30.4 8.959 38.895 3 0.0 1.5

2016 1228 1007 13.0 9.205 38.763 3 0.1 2.1

2016 1230 0810 45.8 8.773 38.642 3 0.2 1.8

2016 1230 0922 21.6 8.953 38.984 3 0.2 2.5

2016 1231 0747 56.3 8.961 38.885 3 0.1 1.6

2017 1 1 0610 43.8 9.798 39.896 3 0.1 4.7

2017 1 1 0652 38.7 9.822 39.885 4 0.2 2.9

2017 1 4 0915 13.1 8.841 38.819 3 0.5 1.7

2017 1 4 1245 32.8 8.919 38.917 3 0.3 1.7

2017 1 5 0325 3.8 9.124 39.814 4 1.3 3.3

2017 1 5 0721 7.3 8.995 38.903 3 0.2 2.0

2017 1 5 2348 7.4 9.818 39.889 4 0.3 2.2

2017 111 0300 59.6 9.194 38.918 3 0.3 2.8

2017 111 0823 46.1 8.670 38.715 3 0.2 2.0

2017 111 0950 58.3 8.818 38.592 3 0.2 1.7

2017 112 0817 13.2 8.896 39.064 3 0.1 2.2

2017 114 0906 31.8 8.973 38.918 3 0.0 2.2

2017 114 1336 35.1 8.923 38.905 3 0.2 1.8

2017 115 0801 26.2 8.931 38.842 3 0.2 1.3

2017 115 1347 27.0 9.825 39.888 4 0.2 3.2

2017 116 0828 33.0 9.843 39.746 4 0.2 2.6

2017 116 1139 3.1 8.978 38.931 3 0.0 1.9

2017 121 1009 22.1 8.843 38.593 3 0.8 2.0

2017 123 0745 56.8 9.000 38.896 3 0.1 1.7

2017 124 1324 15.6 8.909 38.917 3 0.3 1.6

2017 125 2245 49.2 9.504 39.474 3 0.2 1.6

2017 126 0857 1.8 9.299 39.098 4 0.2 2.0

2017 126 1155 24.8 9.007 38.929 3 0.2 1.7

2017 126 1320 30.1 9.035 38.956 3 0.3 2.0

2017 127 1153 51.0 9.290 39.695 3 0.4 2.7

2017 2 4 0751 48.2 8.822 38.601 3 0.1 1.4

2017 2 4 1110 15.0 8.826 38.751 3 0.2 1.9

2017 2 4 1216 43.0 9.196 38.751 3 0.2 1.9

2017 2 5 0800 42.5 8.713 38.657 3 0.1 1.7

2017 2 6 1136 48.2 8.958 38.892 3 0.0 1.9

2017 2 6 1136 48.0 8.953 38.893 3 0.1 1.6

2017 2 6 1307 32.5 8.980 38.928 3 0.2 2.1

2017 2 7 0629 48.7 8.974 38.913 3 0.2 1.9

2017 2 7 1250 56.2 8.920 38.974 3 0.2 2.1

2017 2 9 0815 15.8 8.955 38.958 3 0.3 1.9

2017 210 0717 35.1 9.022 38.956 3 0.1 2.5

2017	210	0837 39.9	9.041	38.932	3	0.2	2.0
2017	211	0136 45.1	9.513	40.043	4	0.2	2.6
2017	211	0146 24.1	9.811	39.858	4	0.6	2.5
2017	211	0828 56.8	8.995	38.929	3	0.2	2.1
2017	212	1834 1.4	9.817	39.894	4	0.2	3.4
2017	212	1915 2.3	9.556	40.043	4	0.2	3.2
2017	213	0911 0.3	8.952	38.908	3	0.0	2.3
2017	213	1035 3.2	8.845	38.775	3	0.2	2.3
2017	215	1231 9.5	8.969	38.925	3	0.1	2.4
2017	216	0747 46.1	9.017	38.914	3	0.1	2.0
2017	216	1053 26.1	8.730	38.669	3	0.1	1.4
2017	216	1133 42.8	8.916	38.845	3	0.0	1.7
2017	217	0040 0.9	9.561	40.026	4	0.3	3.0
2017	218	0951 38.9	8.978	38.914	3	0.2	1.9
2017	219	1229 25.1	9.182	38.532	3	0.2	2.0
2017	220	2319 21.8	9.736	39.330	4	0.2	2.6
2017	223	0656 45.5	8.766	38.566	3	0.1	1.8
2017	224	0821 25.4	8.834	38.614	3	0.1	1.7
2017	225	0717 31.0	8.982	38.903	3	0.2	1.6
2017	225	0743 28.8	8.822	38.592	3	0.1	1.7
2017	226	0946 38.8	8.913	38.474	3	0.2	2.0
2017	227	1100 1.9	8.907	38.502	3	0.1	1.8
2017	228	0728 59.7	8.970	38.908	3	0.1	1.9
2017	3 3	0709 26.8	9.007	38.890	3	0.0	1.8
2017	3 3	0721 55.8	9.000	38.906	3	0.1	1.8

2017	3 4	1117	27.6	9.137	39.800	4	1.4	3.0
2017	3 4	1217	29.2	9.200	38.753	3	0.1	1.3
2017	3 5	0455	42.5	9.520	40.013	4	0.8	3.0
2017	3 5	0824	38.7	8.951	38.860	3	0.1	1.8
2017	3 6	0757	39.9	9.006	38.893	3	0.0	1.9
2017	3 8	0650	8.4	8.969	38.892	3	0.1	1.3
2017	3 8	0934	52.4	8.832	38.665	4	0.3	2.2
2017	3 9	0717	16.4	8.987	38.911	3	0.3	1.7
2017	3 9	0745	43.1	8.877	38.862	3	0.1	1.9
2017	310	0720	40.4	9.012	38.974	3	0.1	2.3
2017	310	0735	13.0	8.716	38.686	3	0.1	2.1
2017	314	0601	10.4	9.770	39.898	4	0.3	3.2
2017	314	1201	22.4	8.777	38.621	3	0.0	2.1
2017	315	0712	10.1	9.039	38.895	3	0.2	1.6
2017	315	0839	28.1	8.821	38.753	3	0.0	1.8
2017	315	1002	44.2	8.957	38.890	3	0.1	1.7
2017	315	1005	9.3	9.192	38.639	3	0.2	2.0
2017	318	0842	13.7	8.973	38.907	3	0.0	1.9
2017	318	1053	14.3	9.203	38.755	3	0.1	1.9
2017	318	1125	7.2	9.231	38.787	3	0.1	2.3
2017	320	1302	27.7	9.020	38.944	3	0.3	2.7
2017	321	1219	48.1	8.914	38.503	3	0.2	2.2
2017	322	1006	6.8	8.817	38.628	3	0.3	1.8
2017	323	1000	59.1	8.968	38.918	3	0.2	1.5
2017	325	0633	53.0	8.993	38.890	3	0.2	1.2

2017	325	0708	26.4	8.773	38.591	3	0.3	1.6
2017	325	0835	37.2	8.953	38.922	3	0.1	2.0
2017	325	1057	55.3	8.914	38.897	3	0.1	1.4
2017	326	1101	27.4	8.971	38.920	3	0.1	2.2
2017	414	0731	52.0	9.027	38.963	3	0.1	2.2
2017	419	0909	28.0	9.026	38.900	3	0.3	1.3
2017	426	0707	25.0	8.994	38.862	3	0.3	1.2
2017	426	1058	53.6	8.945	39.067	3	0.2	2.4
2017	427	0645	8.4	8.975	38.920	3	0.2	2.0
2017	427	0925	55.6	9.005	38.921	3	0.1	1.4
2017	427	1007	49.8	9.012	38.950	3	0.3	1.7
2017	5 3	1046	22.3	8.834	38.753	3	0.1	1.7
2017	5 4	0933	56.0	8.833	38.908	3	0.2	1.3
2017	512	0932	40.0	8.903	38.616	3	0.0	1.8
2017	513	0715	34.3	8.971	38.893	3	0.0	1.4
2017	513	1010	55.7	8.966	38.934	3	0.1	1.9
2017	520	1253	22.4	8.919	38.502	3	0.3	2.1
2017	523	1652	27.6	9.561	40.041	3	0.3	2.7
2017	525	0810	23.5	8.823	38.551	3	0.3	1.9
2017	526	1049	38.8	9.090	39.154	3	0.2	2.4
2017	527	1004	34.2	9.065	39.241	3	1.8	2.3
2017	6 5	1021	57.5	8.901	38.465	3	0.7	1.8
2017	6 6	0812	36.6	8.861	38.530	3	0.0	1.8
2017	6 9	1004	36.9	9.006	38.952	3	0.4	1.3
2017	612	1002	59.9	8.829	38.729	3	0.1	1.9

2017	617	2147	20.2	9.977	45.793	3	0.6	4.1
2017	619	0954	46.0	8.974	38.898	3	0.0	2.0
2017	620	0949	7.0	8.865	39.027	3	0.3	2.4
2017	630	0745	1.7	9.002	38.887	3	0.0	1.9
2017	7 1	0814	56.5	8.732	38.703	3	0.0	1.8
2017	714	0753	42.4	8.818	38.552	3	0.2	1.6